Title

Comparative analysis of SN 2012dn optical spectra: days −14 to +114

Journal

Monthly Notices of the Royal Astronomical Society, 457(4)

ISSN

0035-8711

Authors

Parrent, JT
Howell, DA
Fesen, RA
et al.

Publication Date

2016-04-21

DOI

10.1093/mnras/stw239

Peer reviewed

Monthly Notices of the ROYAL ASTRONOMICAL SOCIETY

MNRAS **457,** 3702–3723 (2016) doi:10.1093/mnras/stw239
Advance Access publication 2016 January 29

Comparative analysis of SN 2012dn optical spectra: days −14 to +114

J. T. Parrent,[1,2,3★] D. A. Howell,[2,4★] R. A. Fesen,[3] S. Parker,[5] F. B. Bianco,[6] B. Dilday,[7] D. Sand,[8] S. Valenti,[2,3] J. Vinkó,[9,10] P. Berlind,[11] P. Challis,[1] D. Milisavljevic,[1] N. Sanders,[1] G. H. Marion,[10] J. C. Wheeler,[10] P. Brown,[12] M. L. Calkins,[6] B. Friesen,[13] R. Kirshner,[1] T. Pritchard,[14] R. Quimby[15,16] and P. Roming[14,17]

[1]*Harvard–Smithsonian Center for Astrophysics, 60 Garden St, Cambridge, MA 02138, USA*
[2]*Las Cumbres Observatory Global Telescope Network, Goleta, CA 93117, USA*
[3]*6127 Wilder Lab, Department of Physics and Astronomy, Dartmouth College, Hanover, NH 03755, USA*
[4]*Department of Physics, U.C. Santa Barbara, Santa Barbara, CA 93117, USA*
[5]*Backyard Observatory Supernova Search, Parkdale Observatory, Canterbury 7495, New Zealand*
[6]*Center for Cosmology and Particle Physics, New York University, 4 Washington Place, New York, NY 10003, USA*
[7]*Gravity Jack, 23505 E Appleway Ave #200, Liberty Lake, WA 99019, USA*
[8]*Physics Department, Texas Tech University, Lubbock, TX 79409, USA*
[9]*Department of Optics and Quantum Electronics, University of Szeged, Dóm tér 9, 6720 Szeged, Hungary*
[10]*Department of Astronomy, University of Texas, Austin, TX 78712, USA*
[11]*F. L. Whipple Observatory, 670 Mt Hopkins Road, PO Box 97, Amado, AZ 85645, USA*
[12]*Department of Physics and Astronomy, George P. and Cynthia Woods Mitchell Institute for Fundamental Physics and Astronomy, Texas A. & M. University, 4242 TAMU, College Station, TX 77843, USA*
[13]*Homer L. Dodge Department of Physics and Astronomy, University of Oklahoma, 440 W Brooks, Norman, OK 73019, USA*
[14]*Department of Astronomy and Astrophysics, Penn State University, 525 Davey Lab, University Park, PA 16802, USA*
[15]*Department of Astronomy, San Diego State University, 5500 Campanile Drive, San Diego, CA 92182-1221, USA*
[16]*Kavli IPMU (WPI), UTIAS, The University of Tokyo, Kashiwa, Chiba 277-8583, Japan*
[17]*Southwest Research Institute, Department of Space Science, 6220 Culebra Road, San Antonio, TX 78238, USA*

Accepted 2016 January 27. Received 2016 January 27; in original form 2015 May 31

ABSTRACT

SN 2012dn is a super-Chandrasekhar mass candidate in a purportedly normal spiral (SAcd) galaxy, and poses a challenge for theories of type Ia supernova diversity. Here we utilize the fast and highly parametrized spectrum synthesis tool, SYNAPPS, to estimate relative expansion velocities of species inferred from optical spectra obtained with six facilities. As with previous studies of normal SN Ia, we find that both unburned carbon and intermediate-mass elements are spatially coincident within the ejecta near and below 14 000 km s^{-1}. Although the upper limit on SN 2012dn's peak luminosity is comparable to some of the most luminous normal SN Ia, we find a progenitor mass exceeding ∼1.6 M$_\odot$ is not strongly favoured by leading merger models since these models do not accurately predict spectroscopic observations of SN 2012dn and more normal events. In addition, a comparison of light curves and host-galaxy masses for a sample of literature and Palomar Transient Factory SN Ia reveals a diverse distribution of SN Ia subtypes where carbon-rich material remains unburned in some instances. Such events include SN 1991T, 1997br, and 1999aa where trace signatures of C III at optical wavelengths are presumably detected.

Key words: supernovae: general – supernovae: individual: SN 2012dn.

1 INTRODUCTION

The progenitor systems of type Ia supernovae (SN Ia) have not been observed, although it is widely believed that some SN Ia are the product of a thermonuclear runaway in a white dwarf (WD) star with a mass near the Chandrasekhar limit, $M_{\rm Ch} \approx 1.38$ M$_\odot$ (Nugent et al.

★ E-mail: jparrent@cfa.harvard.edu (JTP); ahowell@lcogt.net (DAH)

2011 and references therein). There is also observational evidence to suggest that the progenitor mass for a fraction of overluminous events may exceed $M_{\rm Ch}$ (Howell et al. 2006; Jeffery, Branch & Baron 2006; Yamanaka et al. 2009; Scalzo et al. 2010), while the progenitor mass for some fraction of normal and sub-luminous SN Ia may be notably less than $M_{\rm Ch}$ (Woosley & Kasen 2011; Scalzo, Ruiter & Sim 2014c; Shen & Moore 2014; Dan et al. 2015).

Studies of SN Ia therefore face an interesting challenge as these exploded WD systems may be the merger of two sub-$M_{\rm Ch}$ WDs (Kromer et al. 2013), some involving low-mass helium stars (Shen & Moore 2014; Dan et al. 2015); coalesced mergers or prompt 'peri-mergers' of two near-$M_{\rm Ch}$ WDs (Moll et al. 2014; Raskin et al. 2014); massive WDs in single-degenerate systems (Hachisu et al. 2012; Chen et al. 2014); and single-degenerate systems with sub-$M_{\rm Ch}$ ejecta masses (Chiosi et al. 2015). Spectroscopic modelling has also yet to distinguish appearances between single and double-degenerate scenarios (Liu, Jeffery & Schultz 1997; Kasen & Plewa 2007; Röpke et al. 2012; Dessart et al. 2014; Mazzali et al. 2015). The uniqueness of progenitor systems that produce super-$M_{\rm Ch}$ mass candidates (SCC) and more common SN Ia thus remains an open issue.

Early-phase optical spectra of the SCC class are thus far characterized by relatively weak and narrow spectral features, moderate to low mean expansion velocities (8–16 $\times$ 10^3 km s^{-1}), lower than normal line-velocity gradients of blended absorption minima, and higher than normal integrated flux near maximum light (Scalzo et al. 2012; Brown et al. 2014). This in combination with relatively large and long-lasting signatures of C II $\lambda\lambda$ 6580, 7234suggest the presence of higher than normal amounts of unburned carbon (Howell et al. 2006; Scalzo et al. 2010; Taubenberger et al. 2013). Although there are few well-observed SCC SN Ia, e.g. the overluminous SN 2009dc (Yamanaka et al. 2009; Tanaka et al. 2010; Silverman et al. 2011), the most recent, SN 2012dn, reached a peak absolute magnitude that was not exceptionally luminous (Brown et al. 2014; Chakradhari et al. 2014), and the same can be said for the spectroscopically similar SN 2006gz (Maeda et al. 2009).

For some SCC SN Ia, signatures of C II may not be conspicuous above low signal-to-noise ratios, or the signature may be fast-evolving similar to that seen for the normal, SN 1999aa-like hybrid, SN 2013dy (see also SN 1999ac; Garavini et al. 2005). Signatures of carbon might also be detected as C III λ4649 in so-called Shallow Silicon SN Ia that display spectral signatures of overall higher ionization species, e.g. SN 1991T and 1997br (Hatano et al. 2002; Garavini et al. 2004; Parrent et al. 2011; Zheng et al. 2013; Scalzo et al. 2014b). Seemingly smaller amounts of unburned material of the C+O progenitor, or burned material of the He+C+O progenitor, are frequently detected for so-called Core Normal SN Ia (Jeffery et al. 1992; Fisher et al. 1997; Branch et al. 2005; Thomas et al. 2007), while signatures of C I λ10691 are detected for several events, and possibly all SN Ia (Höflich et al. 2002; Hsiao et al. 2015; Marion et al. 2015).

Signatures of carbon in the outermost ejecta may be a general characteristic of Pulsational-Delayed Detonation(-like) (PDD) explosion mechanisms, as proposed for SN 2011fe and 2013dy-like events (Khokhlov 1991; Bravo et al. 2009; Dessart et al. 2014), in addition to peculiar SN 2002cx-like events (Baron 2014). Carbon-rich regions may also be associated with the remains of a degenerate secondary star that is distributed amorphously at the time of the explosion, where signatures of C II may not be physically associated with C I deeper within the ejecta of the primary WD (cf. Taubenberger et al. 2011, 2013; Moll et al. 2014; Raskin et al. 2014). Adding to this complexity is whether normal SN Ia originate from a sub-Chandrasekhar mass primary WD (Woosley & Weaver 1994; Liu, Jeffery & Schultz 1998; van Kerkwijk, Chang & Justham 2010; Pakmor et al. 2012; Raskin & Kasen 2013; Scalzo et al. 2014c; Chiosi et al. 2015).

From comparisons of synthesized photometry and spectra, Pakmor et al. (2012) found moderate agreement between the normal SN Ia 2003du and their violent merger model totaling 2.0 $M_\odot$ (see also Moll et al. 2014). Raskin et al. (2014) later presented four post-merger models, showing that the angle-dependent, maximum-light spectra of their most normal SN Ia-like 0.9 + 0.8 $M_\odot$ model are not also well-matched to most SN Ia belonging to the SCC class (see also van Rossum et al. 2015). More recently, Dan et al. (2015) reported on their post-merger remnant calculations from an initial sample of nine WD configurations. Out of the three models in fair agreement with spectroscopic abundance estimates of 'normal' SN Ia, the total masses for those models are 1.6 $M_\odot$ and 2.1 $M_\odot$, where the former involves a 0.45 $M_\odot$ helium WD. A common theme for these WD merger models is that the overlap between the bulk of the carbon and intermediate-mass ejecta appears to be dependent on the total progenitor mass and viewing angle.

In terms of observed line velocities, carbon-rich regions of absorbing material for both normal and SCC SN Ia are estimated to be spatially coincident with freshly synthesized intermediate-mass elements, e.g. Mg, Si, S, and Ca (Branch et al. 2005; Hicken et al. 2007). However, the measurable degree of overlap between potentially unburned progenitor material and regions of Mg, Si, and Ca remains uncertain on account of excessive line-blending (van Rossum 2012; Foley 2013; Parrent, Friesen & Parthasarathy 2014). There is also evidence to suggest the presence of multiple high-velocity shells of Ca II in the outermost ejecta (Thomas et al. 2004), which is more than the single high-velocity component typically assumed for surveys of SN Ia spectra (e.g. Silverman et al. 2013; Childress et al. 2014; Maguire et al. 2014; Pan et al. 2015).

In this article we supplement previously collected data and analyse our time series optical observations of SN 2012dn during its photospheric phases, starting approximately 15 d prior to maximum light, with late-time coverage at $\sim$114 d after peak brightness. In Section 2 we present our collected *gri* photometry and optical spectra. In Section 3 we assess the peak absolute magnitude of SN 2012dn and compare to light curves of other SN Ia prototypes. In Section 4 we examine dissimilarities between the spectra of SN 2012dn and literature SN Ia. In Section 5 we outline our approach in utilizing the fast and highly parametrized LTE line-identification tool, SYNAPPS (Thomas, Nugent & Meza 2011a). In Section 6 we analyse the spectra of SN 2012dn with SYNAPPS and discuss our application of a simplified line-identification schema. In Section 7 we overview SN 2012dn within the greater context of SN Ia diversity. In Section 8 we summarize and highlight our findings.

2 OBSERVATIONS

On 2012 July 8 UT an optical transient source with $m_g \lesssim 16$ was discovered at α(J2000) = $20^{\rm h}23^{\rm m}36\overset{\rm s}{.}26$ and δ(J2000) = $-28^\circ16'43\overset{''}{.}4$ by S. Parker of the Backyard Observatory Supernova Search team (BOSS; Bock, Parrent & Howell 2012). We triggered our Gemini-South Target-of-Opportunity programme (GS-2012A-Q-20; PI, D. A. Howell) and obtained a first spectrum of SN 2012dn on July 10 UT, which turned out to be approximately 15 d before it reached peak *b*-band brightness (Parrent & Howell 2012; Brown et al. 2014; Chakradhari et al. 2014). This spectrum showed weak 6100 Å and 8200 Å features, along with a conspicuous 6300 Å signature, that together suggested SN 2012dn to be an SCC SN Ia.

Table 1. FTS photometry for SN 2012dn.

UT Date	MJD 56000+	Phase (d)	SDSS-*g* (mag)	SDSS-*r* (mag)	SDSS-*i* (mag)
2012/07/16	124.8	−8.0	–	14.543 (004)	14.863 (004)
2012/07/18	126.5	−6.3	14.486 (009)	14.381 (004)	14.743 (004)
2012/07/19	127.5	−5.3	14.421 (010)	14.309 (003)	14.697 (004)
2012/07/20	128.6	−4.2	14.331 (010)	14.223 (003)	14.652 (004)
2012/07/21	129.5	−3.3	14.322 (012)	14.199 (005)	14.624 (003)
2012/07/21	129.8	−3.0	14.328 (019)	14.198 (009)	14.594 (004)
2012/07/22	130.5	−2.3	14.297 (012)	14.200 (007)	14.588 (004)
2012/07/24	132.5	−0.3	14.276 (013)	14.085 (004)	14.551 (006)
2012/07/25	133.5	+0.7	14.242 (012)	14.131 (008)	14.574 (004)
2012/07/26	134.7	+1.9	14.249 (012)	14.119 (004)	14.553 (003)
2012/07/28	136.5	+3.7	14.227 (053)	14.116 (011)	14.568 (019)
2012/07/29	137.5	+4.7	14.286 (021)	14.123 (004)	14.566 (005)
2012/07/30	138.5	+5.7	14.282 (021)	14.124 (007)	14.569 (006)
2012/07/31	139.5	+6.7	–	14.203 (009)	–
2012/08/03	142.6	+9.8	14.528 (019)	–	14.548 (007)
2012/08/04	143.5	+10.8	14.492 (012)	14.220 (006)	14.608 (004)
2012/08/05	144.5	+11.8	14.582 (009)	14.255 (004)	14.636 (005)
2012/08/06	145.6	+12.8	14.649 (012)	14.265 (006)	14.617 (004)
2012/08/07	146.5	+13.7	14.690 (015)	14.312 (005)	14.670 (006)
2012/08/09	148.5	+15.7	14.892 (010)	14.399 (004)	14.693 (004)
2012/08/10	149.5	+16.7	14.929 (010)	14.405 (003)	14.695 (004)
2012/08/10	149.7	+16.9	14.951 (014)	14.426 (004)	14.689 (003)
2012/08/11	150.5	+17.7	15.065 (013)	14.443 (004)	14.715 (005)
2012/08/12	151.5	+18.7	15.148 (012)	14.475 (010)	14.738 (007)
2012/08/12	151.7	+18.9	15.176 (012)	14.487 (004)	14.708 (005)
2012/08/13	152.7	+19.9	15.333 (016)	14.518 (007)	14.713 (005)
2012/08/14	153.5	+20.7	15.353 (013)	14.555 (006)	14.737 (005)
2012/08/15	154.5	+21.7	15.425 (020)	14.639 (015)	14.709 (005)
2012/08/16	155.5	+22.7	15.597 (016)	14.601 (010)	14.751 (011)
2012/08/20	159.5	+26.8	15.925 (034)	14.817 (010)	14.869 (013)
2012/08/21	160.5	+27.8	–	14.862 (016)	14.815 (098)
2012/08/24	163.5	+30.7	16.160 (012)	14.988 (005)	14.981 (007)
2012/08/30	169.5	+36.7	16.428 (028)	15.238 (009)	15.212 (007)
2012/08/31	170.7	+37.9	16.458 (061)	15.285 (025)	15.253 (020)
2012/09/01	171.5	+38.7	16.509 (021)	15.298 (006)	15.289 (006)
2012/09/02	172.5	+38.7	16.539 (014)	15.355 (007)	15.395 (008)
2012/09/03	173.5	+40.7	16.590 (016)	15.404 (006)	15.386 (007)
2012/09/04	174.5	+41.7	16.645 (016)	15.432 (007)	15.444 (005)
2012/09/06	176.5	+43.7	16.684 (016)	15.520 (008)	15.491 (006)
2012/09/12	182.4	+49.6	16.836 (021)	15.778 (014)	15.691 (010)
2012/09/19	189.4	+56.6	17.036 (018)	16.030 (015)	16.000 (008)
2012/09/23	193.4	+60.6	17.134 (020)	16.164 (019)	16.129 (012)
2012/09/27	197.4	+64.6	17.355 (051)	16.387 (032)	16.328 (013)
2012/09/28	198.4	+65.6	–	16.313 (128)	16.402 (085)
2012/09/30	200.4	+67.6	17.384 (020)	16.487 (013)	16.560 (010)
2012/10/04	204.4	+71.6	17.656 (033)	16.684 (019)	16.669 (016)
2012/10/17	217.4	+84.6	17.848 (036)	17.204 (022)	17.264 (027)
2013/06/22	465.7	+332.9	20.846 (143)	20.301 (082)	20.805 (111)
2013/06/23	466.6	+333.8	20.953 (195)	20.533 (131)	20.771 (149)
2013/07/07	480.6	+347.8	19.562 (050)	19.668 (055)	20.125 (056)

2.1 Photometry

Photometric observations using *g'r'i'* filters were obtained with the Spectral camera on Faulkes Telescope South (FTS), spanning nearly a year of coverage (see Table 1 and Fig. 1). Our observations began on 2012 July UT 16, about four days after the *Swift*/UVOT photometry of Brown et al. (2014) and Chakradhari et al. (2014). Images and filtered photon counts were processed and converted to SDSS *gri* with an automatic pipeline of standard IRAF procedures (see Graham et al. 2014; Valenti et al. 2014 for details).

2.2 Spectroscopy

Spectroscopic observations of SN 2012dn were obtained by six facilities: Gemini-North and Gemini-South with GMOS (Hook et al. 2004; Howell et al. 2012), South African Large Telescope (SALT) with RSS (Burgh et al. 2003; Nordsieck 2012), Tillinghast Telescope with the FAST spectrograph (Fabricant et al. 1998), Faulkes Telescope South (FTS) with FLOYDS (Brown et al. 2013), and the Multiple Mirror Telescope (MMT) using the Blue Channel instrument (Schmidt, Weymann & Foltz 1989). Data were reduced with

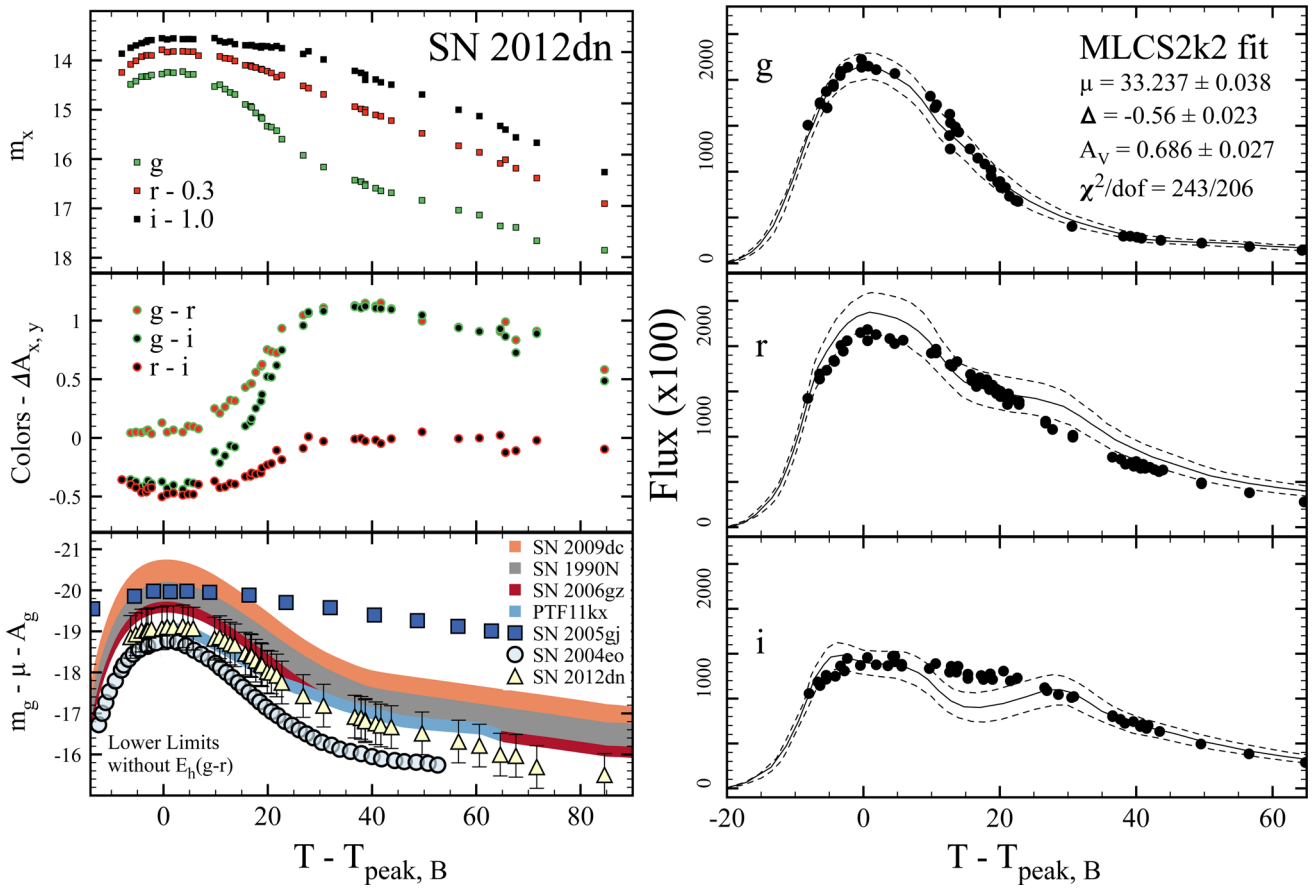

Figure 1. Top-left: FTS *gri* observed magnitudes of SN 2012dn during its first 100 d (accounting for ∼4 d unobserved prior to day −14.6), corrected for MWG extinction, is plotted against MLCS2k2 estimated maximum light (MJD 56132.8). Middle-left: $g-r$, $g-i$, and $r-i$ colours of SN 2012dn. Bottom-left: absolute g-band magnitude estimated comparisons of SN 2012dn from Chakradhari et al. (2014), 2006gz, 2009dc, and Core Normal events. Additional photometry was produced with SNLS software to K-correct light curves of SN 1990N (Lira et al. 1998), 2006gz (Hicken et al. 2007), and 2009dc (Silverman et al. 2011) from B, V, and I band to FTS g, r, and i-band filters in the AB photometric system; here we only plot g-band values. We have supplemented comparisons with light curves for SN 2005gj and PTF11kx (Ia-CSM; Aldering et al. 2006; Prieto et al. 2007; Dilday et al. 2012) and SN 2004eo (an intermediate between normal and SN 1991bg; Pastorello et al. 2007b; Mazzali et al. 2008). Error bounds for comparison light curves are with respect to uncertainties in host galaxy extinction and distance modulus. For clarity, we have omitted photometry points at ∼one year post-maximum light. Right: our MLCS2k2 fit to SN 2012dn gri photometry. Filtered photon counts are given on the y-axis, and the x-axis is the time relative to the date of peak brightness. MLCS2k2 fitting parameters are given in the upper-right panel.

IRAF, including Gemini software add-on packages, and have been corrected for host recessional velocities in all figures assuming a redshift of $z = 0.010\,187$ unless otherwise stated (Theureau et al. 1998).

For several FAST spectra, galaxy contamination is apparent near 6563 Å, and telluric features have not been removed in our data set (as indicated in Fig. 2). We note however that neither of these contaminants have significant effect on our subsequent analysis of SN 2012dn spectra in Section 6.

Assuming SN 2012dn reached b-band maximum light on 2012 July UT 24.8 (Brown et al. 2014), optical spectra of SN 2012dn were obtained from day −14.6 to day +10.2, with a follow-up spectrum taken at +114.2 (see Table 2). In total we collected 15 spectra over the course of its first 25 d since discovery, with spectroscopic details probed out to late post-maximum light phases, and are shown in the observer frame in the left-hand panel of Fig. 2. Complimentary observations extend into post-maximum phases by Chakradhari et al. (2014) who collected 10 additional spectra from day +10.4 to day +98.2, in addition to six photospheric phase spectra.

3 LIGHT CURVES

3.1 Absolute magnitudes

To estimate a date of maximum light, we utilize the multicolour light-curve fitter, MLCS2k2 (Jha, Riess & Kirshner 2007), with our fit shown in the right-hand panel of Fig. 1.[1] We find that SN 2012dn reached B-band maximum light on MJD 56132.8 (2012 July UT 24.8), which is consistent with that found from *Swift*/UVOT broad-band photometry obtained by Brown et al. (2014).

Assuming $A_r^{\rm MWG} = 0.14$ mag (Schlafly & Finkbeiner 2011) and a Tully–Fisher distance modulus $\mu = 33.15 \pm 0.52$ (Springob et al. 2007), an observed peak r-band magnitude of 14.26 implies $M_r^{\rm peak} \approx -19.03$. (Brown et al. 2014 assume $\mu = 33.32 \pm 0.20$ and Chakradhari et al. 2014 use 33.15 ± 0.15.) For g-band estimates, we find $M_g^{\rm peak} = -19.09$ for $A_g^{\rm MWG} = 0.20$ mag.

[1] http://www.physics.rutgers.edu/∼saurabh/MLCS2k2/

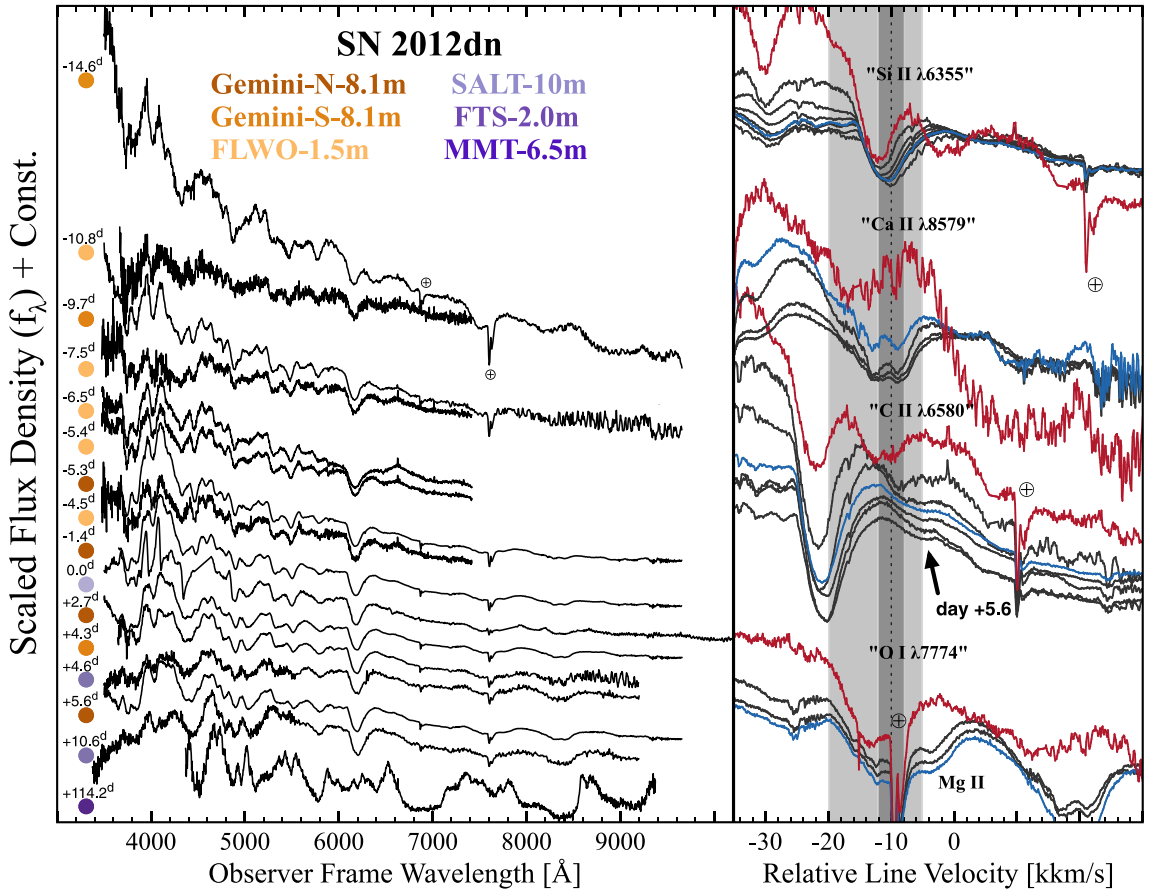

Figure 2. Left: Observer frame spectra for SN 2012dn. Spectra are colored by facilities listed above. Some telluric features are marked by ⊕. See Table 2 for details. Right: Stacked velocity plotted spectra of SN 2012dn pre-maximum light spectra. Spectra are shown with respect to $\mathcal{O}$(v/c) relative line velocities as indicated. See Section 5 where our SYNAPPS analysis includes the relativistic correction term for estimating projected Doppler line velocities for rest-frame spectra. Red and blue lines denote the first and maximum light spectrum, respectively. A vertical dark-grey column centered about 10 000 km s^{-1} is meant to guide the eye for inspecting overlapping line velocities, and the vertical light-grey band spans the approximate width of the 7500 Å feature for reference.

Table 2. Time-series spectra for SN 2012dn.

UT Date	MJD 56000+	Days since *B*-band maximum	Telescope +Instrument	Exp. time (s)	Range (Å)
10/07/12	118.2	−14.6	GS+GMOS	450(×2)	3500–9500
14/07/12	122.0	−10.8	FLWO+FAST	1200	3500–7400
15/07/12	123.1	−9.7	GS+GMOS	450(×2)	3500–9500
17/07/12	125.3	−7.5	FLWO+FAST	870	3500–7400
18/07/12	126.3	−6.5	FLWO+FAST	1200	3500–7400
19/07/12	127.4	−5.4	FLWO+FAST	1800	3500–7400
19/07/12	127.5	−5.3	GN+GMOS	450(×2)	3500–9500
20/07/12	128.3	−4.5	FLWO+FAST	700	3500–7400
23/07/12	131.5	−1.4	GN+GMOS	450(×2)	3500–9500
24/07/12	132.8	0.0	SALT	600	3500–10000
27/07/12	135.5	+2.7	GN+GMOS	200(×2)	3500–9500
29/07/12	137.1	+4.3	GS+GMOS	120(×2)	3500–9500
29/07/12	137.4	+4.6	FTS+FLOYDS	600	3500–9100
30/07/12	138.4	+5.6	GN+GMOS	240(×2)	3500–9500
04/08/12	143.4	+10.6	FTS+FLOYDS	600	3500–9100
16/11/12	247.0	+114.2	MMT+Blue Channel	900	4200–9200

To estimate the intervening host galaxy extinction, we measure and find an upper limit on the equivalent width of a narrow Na D doublet to be $\lesssim 0.30$ Å. Based on a relation from Poznanski, Prochaska & Bloom (2012), we estimate the reddening due to the host, $E(B-V)_{host}$, to be $\lesssim 0.03$ mag. By contrast, Chakradhari et al. (2014) report a colour excess of $E(B-V)_{host} = 0.12$ mag from reportedly resolved Na D doublet measurements of 0.69 and 0.78, respectively. This implies $A_B^{host} = 0.75$ mag and $M_B^{peak} = -19.52$, where uncertainties may be imparted by moderately low-resolution optical spectra. Here we assume $M_B^{peak} \lesssim -19.0\,(m_B - \mu - A_B^{MWG})$. In the case of moderate extinction, $A_B^{host} \sim 0.4$, it follows that $M_B^{peak} \lesssim -19.4$.

We look to compare this with our light-curve fit in Fig. 1, where `MLCS2k2` handles reddening of the intrinsic spectral energy distribution through two parameters, Δ and A_V; Δ is functionally dependent on the colour difference between high and low stretch light curves such that an SN Ia with $\Delta = 1$ (and $A_V = 0$) is redder than in the case of $\Delta = 0$. For SN 2012dn, `MLCS2k2` returns $\Delta = -0.56 \pm 0.02$, which is out of range for the model, but is also indicative of an intrinsically blue event.

To match the observed colours, `MLCS2k2` compensates for $\Delta = -0.56$ by overestimating additional reddening to $A_V = 0.69 \pm 0.03$; because the shape of SN 2012dn's light curves are not normal, `MLCS2k2` returns an overestimate of host extinction, $A_V^{Host} \sim 0.52$. If there were half a magnitude of extinction from the host galaxy of SN 2012dn, one might also expect to have a redder $g - i$ colour at maximum light. Instead, below in Section 3.2 we find the $g - i$ colour of SN 2012dn is bluer than for SN 2006gz and slightly redder than SN 2009dc during the epoch of peak brightness.

We also infer values for host-extinction with the `SALT2.4` light-curve fitter (Guy et al. 2007), and we find them to be roughly consistent with those obtained above with `MLCS2k2`.[2] `SALT2` returns an apparent B-band magnitude of $m_B^{peak} = 14.25 \pm 0.03$. The values obtained for the c parameter (0.24 ± 0.03), which measures the correlation between (intrinsic plus reddened) colour and peak brightness, and the x_1 parameter (1.81 ± 0.07), which describes the correlation between light-curve width and peak brightness, are indicative of $A_V \sim 0.6$ and `MLCS2k2` $\Delta \sim -0.4$ (cf. Kessler et al. 2009).

An additional uncertainty in the magnitude estimate for SN 2012dn is from the distance modulus, where SN 2012dn could have reached a peak luminosity of $M_g \approx -19.67$ ($M_B \approx -19.69$ in B band; Chakradhari et al. 2014). However, even this approximate upper limit on the inferred peak luminosity for SN 2012dn is not far from the luminous end of seemingly spectroscopically 'normal' events such as SN 1995D ($M_B^{peak} \approx -19.66$; Contardo, Leibundgut & Vacca 2000) and 1999ee ($M_B^{peak} \approx -19.85$; Stritzinger et al. 2002).

Unlike `MLCS2k2`, `SALT2` does not return an explicit distance. Therefore, it must be derived from calibration that depends on cosmological parameters. To test systematics, we adopt the two calibrations of Kessler et al. (2009) and Guy et al. (2010) of $\mu = 32.987 \pm 0.112$ and 32.813 ± 0.145, respectively, to obtain $\bar{\mu} = 32.9 \pm 0.1$, which is much lower than $\mu = 33.24$ from `MLCS2k2`. If the distance to ESO 462-16 is indeed shorter, this still implies a peak brightness for SN 2012dn that is lower than expected for its spectroscopic class. Without accounting for reddening from the host, the difference between peak absolute magnitudes inferred from `MLCS2k2` and `SALT2` is ~0.02 magnitudes in the B band.

[2] http://supernovae.in2p3.fr/salt/doku.php

In spite of the uncertain host-galaxy extinction estimate for SN Ia in general (Phillips et al. 2013; Foley et al. 2014a; see also Cikota, Deustua & Marleau 2016), our observations indicate M_g^{peak} for SN 2012dn is not exceptionally luminous, and is in agreement with previous observations of Brown et al. (2014) and Chakradhari et al. (2014). In fact, SN 2012dn's M_g^{peak} is possibly below that for the Core Normal SN 1990N (see Fig. 1).

Assuming negligible host extinction and $M_B^{peak} = -18.77$, the lower limit on the peak luminosity would suggest a relatively broad range of intrinsic luminosities for this spectroscopic subclass and its progenitor systems (Maeda et al. 2009; Scalzo et al. 2010; Brown et al. 2014). Yet by day +330 post-maximum light, SN 2009dc and SN 2012dn decline to absolute B-band luminosities that are approximately half a magnitude greater than SN 2011fe. ($M_B^{09dc} \sim -12.02 \pm 0.19$, Taubenberger et al. 2011; $M_B^{12dn} \sim -12.39 \pm 0.66$, this work and Chakradhari et al. 2014; $M_B^{11fe} \sim -11.57 \pm 0.19$, Munari et al. 2013.)

Whether or not its original system was in excess of M_{Ch}, there are other photometric characteristics to suggest that SN 2012dn is a peculiar member of the SCC SN Ia subclass. Namely, the 1.08 mag decline in the B band 15 d after peak brightness is only slightly less than those for the brighter end of normal SN Ia, e.g. SN 1990N, 1998bu, 2003du, all of which show signatures of C II in the outermost layers. In terms of the empirical light-curve method of Conley et al. (2008), `SiFTO` fits to a light-curve stretch, $s = 1.28$, for SN 2012dn g and r-band light curves. For comparison, $s \sim 0.81$ for SN 2006D; 0.82, 1994D; 0.86, 1996X; 0.91, 2002bo; 0.93, 2002dj; 0.96, 2005cf; 1.03, 2011fe; 1.04, 2003fg; 1.11, 1999aa; 1.26, 2001ay; and $s \approx 1.29$ for 2009dc.

An additional characteristic of SN 2012dn that indicates a non-standard, perhaps SN 2009dc-like origin is the lack of well-pronounced secondary i-band maximum, or less than what is typically observed for spectroscopically normal SN Ia (Chakradhari et al. 2014). Within the context of the width–luminosity relationship (Khokhlov, Mueller & Hoeflich 1993; Phillips 1993; Phillips et al. 1999), the suppression of a secondary maximum is consistent with spectroscopic indications that a relatively late transition from doubly to singly ionized iron-peak elements has occurred (Kasen & Woosley 2007, and see our Section 5). If there is a less pronounced secondary i-band maximum for SN 2012dn, it would have occurred ~10 d or more ahead of 'normal' SN Ia.

3.2 Colours

The UV flux of SN Ia is wildly variable compared to optical counterparts, which has highlighted UV wavelength regions as a capable, albeit challenging probe for physics unseen by optical wavelengths (Kirshner et al. 1993; Wang et al. 2012; Milne et al. 2013; Mazzali et al. 2014). Compared to SN 2009dc, SN 2005cf and other normal SN Ia are typically redder at NUV wavelengths prior to maximum light (Brown et al. 2009, 2010, 2012; Milne et al. 2010), with some fraction of 'carbon-positive' events being relatively bluer at NUV wavelengths (Thomas et al. 2011b; Milne et al. 2013). Brown et al. (2014) report the early UV colours of SN 2012dn-like events are bluer than normal as well.

Plotted in Fig. 3 are our $g-r$, $g-i$, and $r-i$ colours for SN 2012dn, select SCC SN Ia, and several spectroscopically normal SN Ia for reference. Without correcting for dust extinction internal to the host galaxy, the evolution of SN 2012dn's $g-r$ colour-curve during the first month post-explosion is moderately comparable to the Core Normal SN 2005cf ($M_V^{peak} = -19.30 \pm 0.33$) and an SCC,

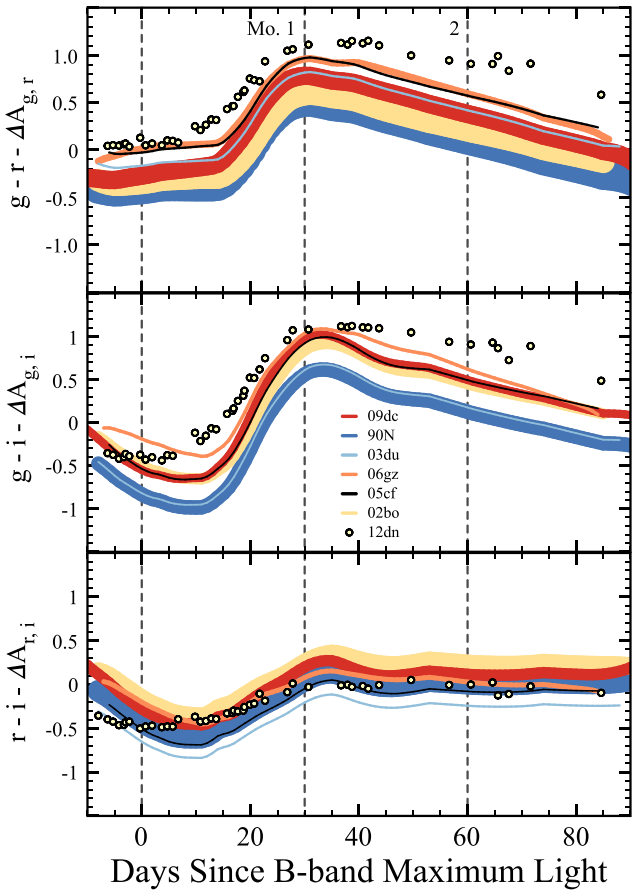

Figure 3. Plotted top–down are $g-r$, $g-i$, and $r-i$ photometric colour comparisons between SN 2012dn (yellow points) and super-Chandrasekhar candidate SN 2006gz and 2009dc, Core Normal SN 1990N, 2003du, and 2005cf, and the Broad Line SN Ia, SN 2002bo (Phillips et al. 1992; Ruiz-Lapuente & Lucy 1992; Benetti et al. 2004; Anupama et al. 2005; Pastorello et al. 2007a; Stanishev et al. 2007; Wang et al. 2009a; Scalzo et al. 2010). Individual colour-curves have not been corrected for reddening from the host-galaxy.

SN 2006gz ($M_V^{\rm peak} = -19.56 \pm 0.18$). The overall $g-r$ colour of SN 2012dn also appears redder than other SN Ia in Fig. 3. Perhaps this is either indicative of significant host-galaxy extinction, which is counter to what we find through equivalent-widths of narrow lines of Na D (Section 3.1), or the overall colour-evolution might suggest a dusty environment local to SN 2012dn (Maeda et al. 2009; Taubenberger et al. 2013). SN 2005cf and 2006gz are also ∼30 per cent redder than the significantly brighter SN 2009dc ($M_V^{\rm peak} = -20.89 \pm 0.54$) on this scale.

We attribute the early departure of SN 2012dn's $g-i$ and $r-i$ colours towards redder values during early post-maximum phases to a relatively slow-declining i-band light curve of 0.01 mag d^{-1} compared to 0.06 mag d^{-1} for g band. Between day +30 and day +85, SN 2012dn's g-band light curve declines by 0.03 mag d^{-1}. SN 2007if underwent a similar decline of ∼0.02 mag d^{-1} on similar time-scales (Scalzo et al. 2010). Compared to Core Normal SN Ia where the decline in g band is also ∼0.03 mag d^{-1}, a relatively hastened late-time decline in brightness is only observed for SN 2012dn at NUV and MUV wavelengths (Brown et al. 2014; Chakradhari et al. 2014).

4 COMPARISON OF SPECTRA

To assess the early spectroscopic evolution and approximate overlap of ejected carbon, oxygen, and select intermediate-mass elements, in the right-hand panel of Fig. 2 we plot the photospheric phase, observer-frame spectra of SN 2012dn in terms of line velocities $\mathcal{O}$(v/c) for Si II λ6355, the Ca II infrared triplet weighted by oscillator strengths (λ8579), C II λ6580, and O I λ7774. For SN 2012dn we find that faster unburned and Si-rich material overlap, in part, below the outer extent of Ca-rich absorbing layers, which is typical for Core Normal SN Ia in terms of singular line velocities. See Section 5 where our SYNAPPS analysis of rest-frame spectra includes the relativistic correction term for estimating projected Doppler velocities.

4.1 Photospheric phases

In the top panel of Fig. 4, comparisons of SN 2012dn to SCCs SN 2006gz, 2007if, and 2009dc during photospheric epochs reveal moderate similarities across optical wavelengths. All share a fairly comparable pseudo-continuum level in addition to superimposed atomic signatures during this phase. Based on dissimilar appearances at blueward wavelengths, one could argue SN 2007if, 2009dc, and 2012dn do not belong to a similar class of events, particularly since too few events have been studied to know which if any is the most normal prototype. Still, while visual comparisons between SN 2012dn and other SCC SN Ia during photospheric phases suggest a match for this subtype, accurate classifications of SN benefit substantially from multi-epoch observations.

4.2 Later phases

In the bottom panel of Fig. 4, we compare late post-maximum spectra of SN 2012dn to a variety of peculiar events. The spectra of SCC SN Ia and SN 2012dn share fairly similar characteristics apart from small line shifts in individual features. It is thus reasonable to suspect that SN 2007if, 2009dc, and 2012dn are of a similar spectroscopic subclass (Brown et al. 2014; Chakradhari et al. 2014).

The moderate contrast between late-time spectra of SN 2012dn, a Core Normal (SN 2011fe), Cool (SN 1991bg), and a more peculiar SN Ia (SN 2002cx; see McCully et al. 2014a,b; Foley et al. 2014b; Stritzinger et al. 2015) suggests SN 2012dn is not strictly 'well-matched' with normal nor historically peculiar SN Ia. In particular, the 4700 and 5900 Å emission line regions of SCC SN Ia are not as prominent compared to that of SN 2011fe, possibly due to relatively sustained heating or less nickel synthesized during the explosion. This might make sense given that SN 1991bg and 2002cx, as subluminous SN Ia, also show less pronounced 4700 Å and 5900 Å features.

5 SEMI-EMPIRICAL LINE IDENTIFICATIONS

For SN spectral features the accuracy of empirical measurements depends on the prescriptions of lines utilized from a supporting abundance model (Hatano et al. 1999a; Branch et al. 2007). Studies of SN diversity thus benefit when prominent detections of select ions can be ruled out. Considering the homogeneous nature of SN Ia spectra, the narrow features of SCC SN Ia lend themselves particularly useful for scrutinizing semi-empirical line-identification schema (e.g. Scalzo et al. 2010; Doull & Baron 2011, and see also Foley et al. 2010a).

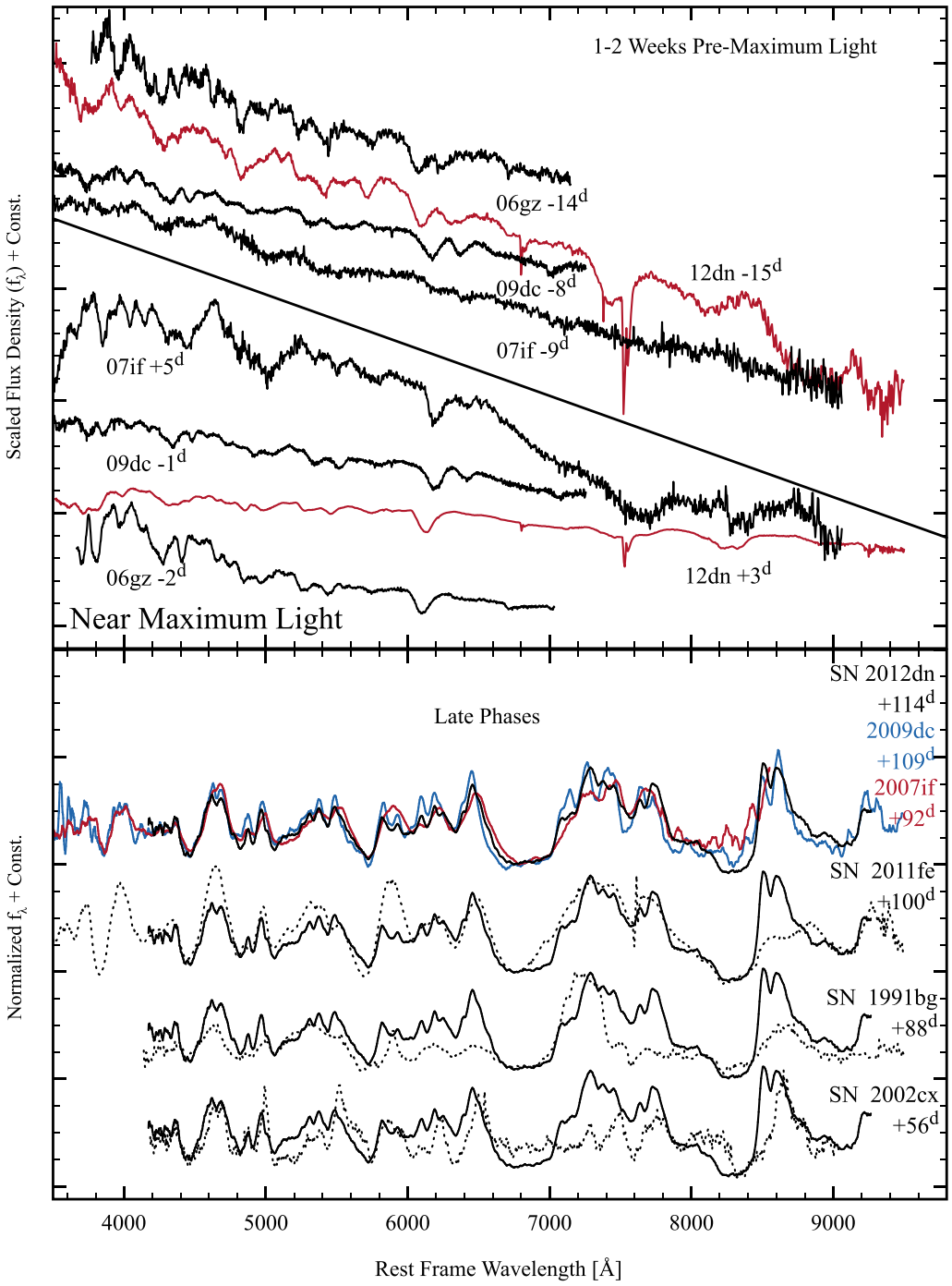

Figure 4. Top: optical spectroscopic comparisons to three super-M_{Ch} candidate SN Ia, 2006gz, 2007if, and 2009dc, during the earliest and near maximum light epochs. Bottom: late post-maximum light phase comparisons of SN 1991bg, 2002cx, 2007if, 2009dc, 2011fe, and 2012dn; SN 1991bg, 2002cx, and 2011fe are the dotted lines.

5.1 The SYNAPPS model

To estimate line velocities of select atomic species, we utilize the fast and highly parametrized spectrum synthesis code, SYNAPPS (Thomas et al. 2011a). The SYNAPPS model, formerly SYNOW (Fisher 2000), assumes spherical symmetry, a sharp photosphere, pure resonance line scattering treated under the Sobolev approximation, and Boltzmann statistics for electron level populations (parametrized by temp in SYNAPPS). For a given reference line, the radial dependence of optical depth is assumed to be an outwardly decreasing exponential that is dependent on the optical depth at the photosphere (logtau), the photospheric velocity (vphot), the detachment velocity for an ion (vmin), and an e-folding parameter (aux). Optical depths of the remaining lines assume LTE level populations.

SYNAPPS essentially views photospheric phase supernova spectra as a non-linear superposition of resonance line P Cygni profiles atop an underlying pseudo-continuum level. While spectrum formation is not similarly trivial for supernova atmospheres (Bongard et al. 2008; Friesen et al. 2014), the one-dimensional SYNAPPS model has served as a complimentary tool to direct comparisons of observed spectra. In certain situations, the rest-wavelength emission component can undergo a similar blueshift, as seen for the absorption component (Baron et al. 1993; Anderson et al. 2014). As the ejecta expands, geometric dilution may cause the rest-wavelength emission to undergo a red-shift during later post-maximum epochs (Friesen et al. 2012). The SYNOW/SYNAPPS model is currently unable to account for these effects on account of an assumed sharp photosphere.

Two of the top-most SYNAPPS parameters are the relative velocities of included ions, v_{min}, and the relative strengths of the lines which can be set by $\log \tau$. By hypothesizing the prescription of lines that influence each composite spectral feature, a synthetic spectrum can be minimized to the data for the available parameter space. For SYNAPPS, this is most often $\log \tau$, v_{phot}, v_{min}, aux, and multiplied by the number of ions included. In turn, this enables a tracing of a monotonically decreasing v_{line} over time ($\pm\, \delta v$; resolutions set by local line-blending).

A reference continuum level is set by an assumed blackbody (T_{BB} in SYNOW; t_{phot} in SYNAPPS). Spectral energy distributions of SN I are not well-represented by blackbodies (Bongard et al. 2006, 2008) and the same can be said for SN II (Hershkowitz, Linder & Wagoner 1986b,a; Hershkowitz & Wagoner 1987). However, the assumption for SYNAPPS is one of practicality and is not meant to be a reliable indicator of a real temperature structure (see fig. 5 of Bongard et al. 2008). In SYNAPPS, quadratic warping constants a_0, a_1, and a_2 supplement t_{phot} to form a more flexible continuum reference level; a_0, a_1, a_2, and t_{phot} form the backbone to data-driven minimization. (See Thomas et al. 2011a and fig. 2 of Parrent et al. 2012 for an example.)

Thus, for well-observed events, one can conduct various experiments to directly assess: (i) detectable and inferable lines of noteworthy species, including C, O, Mg, Si, S, Ca, Fe, and Co at photospheric (PV) and higher velocities (HV); (ii) how to best utilize and constrain semi-empirical line-measurements; (iii) the overlap of burned and remaining progenitor material in terms of line velocities; (iv) the emergence, cutoff, and detachment velocities of select species; (v) the time-dependent prescription and related uncertainties for several composite features (Scalzo et al. 2014b; Milisavljevic et al. 2015); and (vi) line-velocity gradients and plateaus.

5.2 Application of SYNAPPS

Representative 'best fits' to spectra using SYNAPPS are typically initialized by exploring single and multi-ion comparisons while perturbing the available parameters. As mentioned above, because parametrized expansion velocities, v_{line}, are traced by blended atomic signatures over time, the convergence of $v_{min,\,Y}(t)$ with SYNAPPS depends on the list of actively contributing atomic species used as input. However, since SYNAPPS does not solve for ionization balance, which is a necessary step for abundance determinations and more detailed analysis (Baron et al. 1996), semi-empirical fits are devised by perturbing compositional constructs (Hatano et al. 1999a). Synthetic fits for a given set of ions can then be processed forward and backward in phase space relative to maximum light.

The mode of interpretation utilized by SYNAPPS is one of an onion shell paradigm for the radiation transport in supernova atmospheres, which is innately limited (cf. Blondin, Dessart & Hillier 2015). However, the SYNOW model can be used to constrain the compositional structure of ejected material in spite of being confined to Saha–Boltzmann statistics (Branch et al. 2007; Parrent, Branch & Jeffery 2010). A standard prescription of ions for SN Ia stems from Hatano et al. (1999a,b) and Branch et al. (2005), which is based on the time-dependent inclusion of ions including C II, O I, Mg II, Si II, Si III, S II, Ca II, Cr II, Fe II, Fe III, and Co II.

Previously, Branch (1977) showed how the location of an absorption minimum does not always correspond to the model photospheric velocity. This was found to occur for both weak and saturated lines. To ensure minimal under and overshooting in v_{min} for each spectrum of SN 2012dn (and similarly for SN 2011fe in Parrent et al. 2012), we re-examined our preliminary results for a range of saturated optical depths for each ion. Additionally, when v_{min} for any ion was found to be off by more than 1000 km s^{-1} (a common occurrence for Fe II, Fe III, and HV signatures), we perturbed v_{min} by $\pm$ 1000 km s^{-1}, and repeated the above fitting methodology for the entire data set. In the event that the fitting procedure produced either monotonically increasing $v_{min,\,Y}$ over time, or oscillatory solutions with amplitudes exceeding 1000 km s^{-1}, we interpreted this as an artefact of adjacent and unaccounted for lines, $v_{min,\,Z}(t)$, rather than blueward shifting absorption signatures during a period of photospheric recession (Branch & Patchett 1973; Kirshner et al. 1973).

Because we are interested in extracting best estimates of v_{min} for various species, we initially fixed aux and temp at default values of 10^3 km s^{-1} and 10^4 K, respectively, for all but Ca II where we allowed aux to take on values greater than 1000 km s^{-1} (see Branch et al. 2005). These parameters were then free to vary near the end of our fitting procedure. We also allowed logmin to vary freely within appropriate ranges when minimizing $v_{min,\,Y}$ towards a monotonically decreasing function of time (see Hatano et al. 1999a; Branch et al. 2005).

Hence, we define 'best fits' as satisfying the condition that a fit starting with iron-peak elements converge to a similar consensus in $v_{min,\,Y}$ for a fit ending with the inclusion of iron-peak elements (i.e. v_{min} to within 1000 km s^{-1} for each ion considered). With approximately three to five seconds per output spectrum on average, the above vetting process yields on the order of 1–2 $\times$ 10^3 synthetic spectrum comparisons before $v_{min,\,Y}(t)$ begins to converge towards a global minimum in the available parameter space.

6 SPECTRAL ANALYSIS AND RESULTS

In this section we discuss a breakdown of our results, which are shown in Figs 5–10 and later Fig. 13 in Section 7.

6.1 Photospheric velocities of C II

Owing in part to a lack of strong evidence for signatures of high-velocity features compared to more normal SN Ia, the approximate rate of change in line velocities is reportedly lower than normal for SCC SN Ia. None the less, both SN 2006gz and 2012dn have photospheric velocities typical of normal SN Ia despite narrower than normal spectral features (see fig. 20 of Chakradhari et al. 2014). During early photospheric phases, our analysis indicates line velocities of $\sim$14 000 km s^{-1} for Si II. From day $-$14.6 to day +5.6, line velocities are consistent with having only reduced by 2000–3000 km s^{-1} to 11 000–12 000 km s^{-1} (cf. Fig. 5 and 6).

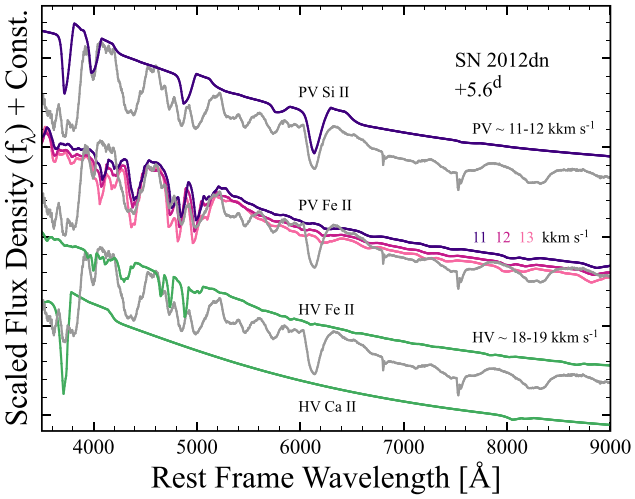

Figure 5. Plotted alongside the day +5.6 spectrum of SN 2012dn (in grey) are single-ion SYN++ synthetic spectra for photospheric Si II and Fe II, in addition to detached, high-velocity Ca II and Fe II. We have exaggerated the strength of HV Ca II lines with SYN++ to show the weak infrared triplet signature. See text in Section 6.2. Model v_{min} are given in units of km s^{-1} 1000^{-1}.

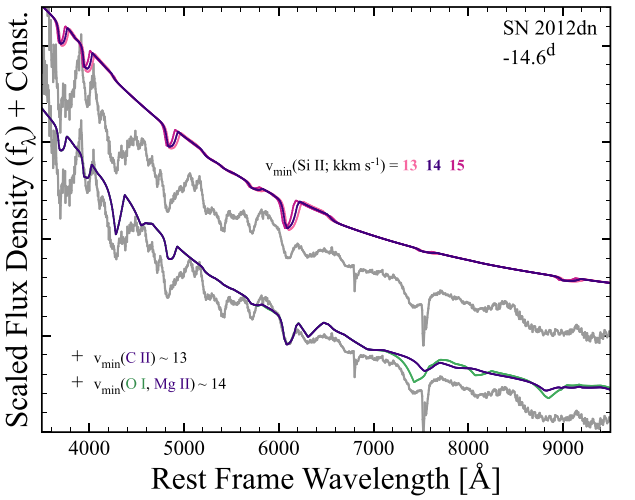

Figure 6. Representative composite SYN++ spectra for Si II, C II+Mg II+Si II, and a single-ion spectrum of O I compared to the day −14.6 of SN 2012dn (in grey). Flux scale is arbitrary and model v_{min} are given in units of km s^{-1} 1000^{-1}. Unlike for Gaussian fitting methods and pseudo-equivalent widths of blended spectral features, the plus symbols here and for the remaining figures do not imply that line formation for SYNAPPS is treated as linearly additive.

Representative single-ion spectra of C II, O I, and Si II are compared to SN 2012dn on day −14.6 in Fig. 6. For C II, the value of v_{min} that our full time series fitting converges towards is slightly below that estimated for Si II (12 000–13 000 km s^{-1} and 14 000–15 000 km s^{-1}, respectively) and is outside typical resolutions for v_{min} of ∼500–1000 km s^{-1}; i.e. we confirm that an improved estimate of v_{min} for C II is not precisely 14 000 km s^{-1}, which is consistent with an independent SYNOW analysis by Chakradhari et al. (2014). If such low projected Doppler velocities reflect ejecta asymmetries, the slight mismatch with v_{min} for Si II could be due to an off-centre distribution of carbon.

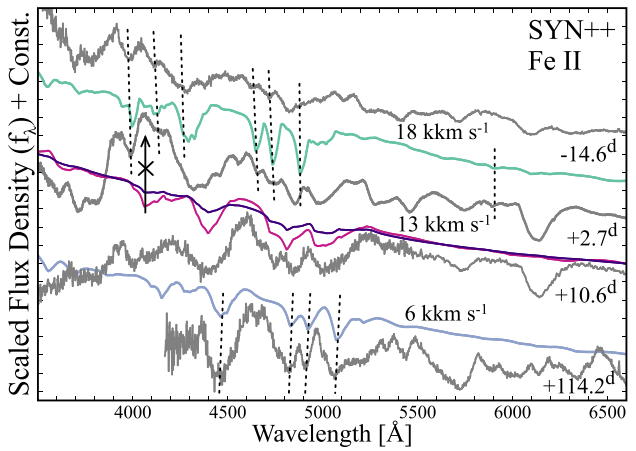

Figure 7. SYN++ single ion comparison for Fe II at 6000, 13 000, and 18 000 km s^{-1}. At post-maximum light phases (after day +10.6), Fe II overlaps nicely with the observed spectrum as a species formed near the photospheric line-forming region. At early epochs (day −14.6), high-velocity Fe II is a promising match. The arrow marked with × signifies that contributions from Fe II are restricted by the data at this wavelength for the given v_{min}.

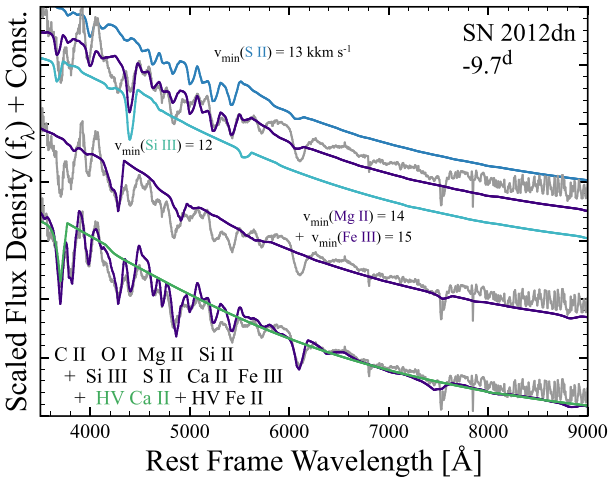

Figure 8. Single-ion and full fit comparisons to the day −9.7 spectrum of SN 2012dn (plotted three times in grey for clarity). Model v_{min} are given in units of km s^{-1} 1000^{-1} and 'HV' denotes detached species at higher than photospheric v_{min}.

Finally we caution that lines of Fe II and Co II are available for contaminating weak 6300 Å features by early post-maximum light phases, thereby further motivating the tracing of time-varying inferences of Fe II. However, by estimating P Cygni summation of Cr II and Co II in the NUV (Scalzo et al. 2010, 2014b; Brown et al. 2014), it is possible to provide a soft upper limit to the blended strength of Fe II and Co II that are permissible near 6300 Å (see Section 6.2 below).

6.2 Direct inference of detached species

From the epoch of maximum light onward, lines of Fe II are expected to influence a number of features at optical wavelengths

(cf. Fig. 5 and fig. 2 of Parrent et al. 2012). However, while small contribution from Fe II can be inferred near day +5.6, Fe II has yet to create a conspicuous and therefore traceable signature during earlier phases. This interpretation is marginally consistent with the lack of a well-pronounced *i*-band double peak for SN 2012dn (Kasen 2006; Chakradhari et al. 2014).

We interpret the lack of obvious Fe II signatures from an incompatible match for the 4100 Å feature between the model Fe II and observations (see Fig. 7); i.e. prior to maximum light, the evolution of SN 2012dn's spectra do not reveal signatures of Fe II that can be easily distinguished from other species like Si II, Si III, S II, S III, and Fe III. Still, this particular 'non-detection' of PV Fe II does not remove (PV + HV) Fe II from influencing the spectrum during this epoch. Rather, the overall structure of the spectrum is difficult to reconcile for a standard prescription of PV Fe II as prescribed with LTE SYNAPPS.

Ultimately, the inference of high-velocity iron-peak elements is currently best served via more detailed modelling. However, to see more clearly when and where lines of (PV + HV) Fe II sync with SN 2012dn spectra, in Fig. 7 we show synthetic single-ion spectra of Fe II for v_{min} set to 18 000, 13 000, and 6000 km s^{-1} and compare them, respectively, to the day −14.6, near-maximum light, and late-time spectra of SN 2012dn.[3] During early 'nebular' phases, the presence of permitted Fe II lines would be most consistent near 6000 km s^{-1}.

If weak signatures of detached HV Ca II and Fe II are present in the spectra of SN 2012dn, then their respective signatures would be consistent with observations assuming line velocities above 18 000 km s^{-1} on day +5.6 and earlier (see Fig. 5). Earlier on day −9.7, the strength of a 4000 Å absorption feature, which is significantly influenced by Si II λ4131, is noticeably larger than normal (see out Fig. 8). This would suggest the relative strengths of PV Si II λλ3858, 4131 could be utilized to rule out faint signatures of detached HV Ca II (see also section 5.4 of Blondin et al. 2013).

To evaluate the potential influence of permitted lines of Fe II and Co II on longer lasting 6300 Å features during post-maximum epochs, in Fig. 9 we examine the day +10.6 spectrum of SN 2012dn. Our full representative fit (in purple) also includes photospheric O I, Mg II, Si II, and Ca II. Line velocities of O I are poorly constrained due to an obscuring telluric feature; however, during these epochs O I is expected to be near line velocities of Si II. (This is also shown in Fig. 6.) By this time, permitted lines of Fe II are consistent with observations for v_{min} near 11 000 km s^{-1}.

When we add Cr II and Co II, the fit (in orange) undergoes a modest improvement bluewards of 4100 Å. Without high signal-to-noise UV coverage, however, we are unable to push spectroscopic interpretations beyond generalizing the presence of iron-peak elements. Therefore, while we suspect 6300 Å features are susceptible to contamination by permitted signatures of Cr II and Co II during post-maximum phases, we cannot precisely investigate the matter here.

6.3 Composite features near 4110 and 4550 Å

The origins of the notches near 4110 Å and 4550 Å in early SN Ia spectra have been difficult to determine on account of excessive line-blending from several candidate ions. For example, it would seem reasonable to associate both of these features with C II λ4267 and λ4743, respectively. In Fig. 6, we show the close proximity of P Cygni profiles C II λ4267 to 4110 Å and C II λ4743 to 4550 Å. It would be advantageous if these features were signatures of unburned progenitor material, particularly when both features in question are in most SN Ia pre-maximum spectra for most SN Ia subtypes (see figs 5–8 in Parrent et al. 2014).

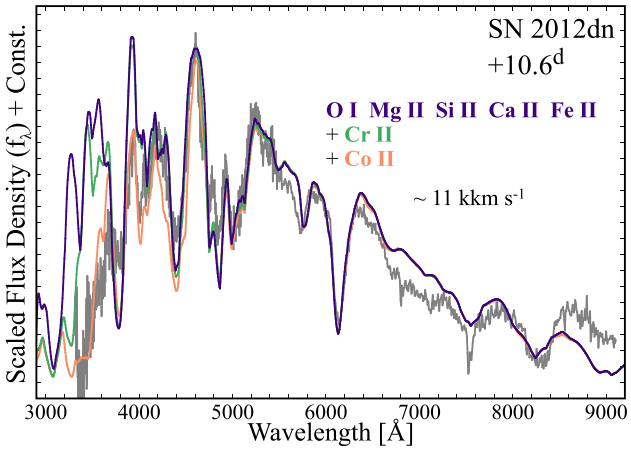

Figure 9. Composite synthetic spectra compared to the day +10.6 spectrum of SN 2012dn (in grey). Model v_{min} are given in units of km s^{-1} 1000^{-1}. Na I has not be included in the fit, and forbidden lines of, e.g. Co III are not taken into account (see Childress et al. 2015).

Whatever the source during photospheric phases, identifying the 4110 Å and 4550 Å notches as primarily indicative of C II line-strengths, however, is not an accurate interpretation, or at least not for SYNAPPS/SYNOW. A possible source for the confusion of 4550 Å features as resulting from C II λ4743 is fig. 1 of Hicken et al. (2007) where the spectrum of SN 2006gz has been imprecisely labeled for this particular feature. Belo we show that the corresponding SYNOW fit is not in fact able to confidently associate C II λλ4267, 4743 with the 4110 Å and 4550 Å features.

6.3.1 *The 4550 Å feature*

At the top of Fig. 8 we compare SYNAPPS single-ion Si III and S II spectra to the day −9.7 spectrum of SN 2012dn. Several narrow features are largely consistent with being shaped, in part, by S II during these photospheric phases. When v_{min} and log τ for S II are adjusted to reproduce the 'S II W', overlap with the 4550 Å feature is obtained without an *ad hoc* tuning of the remaining SYNAPPS parameters. Therefore, rather than C II λ4743, we suspect the 4550 Å feature is instead at least S II, with every other adjacent line influencing the blended strength of S II (including C II λ4743 just barely redwards of the 4550 Å notch).

Even when viewing the post-explosion common envelope or disc region for select super-M_{Ch} merger models, the intensity minimum of a conspicuous C II λ4732 signature is assuredly redwards of the 4550 Å features, and particularly when the associated C II λ6580 is less conspicuous (Raskin et al. 2014). If one were to use SYNAPPS and force the C II to match the 4550 Å feature, then C II λ6580 would not match to the 6300 Å feature; i.e. the accompanying C II λ6580 signature does not hide well in the neighbouring Si II feature for v_{min} = 15 000 km s^{-1} (Parrent et al. 2011), nor is this scenario expected for Broad Line SN Ia (Stehle et al. 2005; Blondin et al. 2015).

One can also argue against C II λ4743 since the 4550 Å feature shows up in the spectra of most SN Ia subtypes during pre-maximum

[3] See also Hatano et al. (1999b) and Branch et al. (2005) who investigated signatures of HV Fe II in the normal SN Ia 1994D.

epochs. How then can near carbon-less SN Ia (e.g. SN 2002dj, 2010jn; Hachinger et al. 2013) still have a near-identical 4550 Å feature? Instead, we suspect the feature may be primarily influenced by S II in those cases as well.

If we instead consider SN 2009dc, an extreme example where the C II λ6580 is more conspicuous than normal, why does the weak 4550 Å not also follow this trend if it is attributed to C II λ4743? Our guess here would at least favour S II, with possibly some contribution from C II near the red-most wing of the 4550 Å feature (see Fig. 8).

From our SYNAPPS analysis, it is reasonable to suspect that the 4550 Å region is also influenced by lines of Si III and Fe II that show up bluewards of 4550 Å (see Figs 6 and 8). That is, the stronger than normal feature immediately bluewards of the 4550 Å notch is not well-matched by C II λ4743, nor is it necessarily available. Better agreement is found with Si III λ4560, which we suspect is then influenced proportionately by Fe II over time. An interpretation of Si III is reasonable considering the time-dependent presence of an equally tentative detection of Si III on the red-most side of the 'S II W' (Thomas et al. 2007; Hachinger et al. 2012; Sasdelli et al. 2014; and see our Fig. 8 and Section 6.4). This appears to be consistent with the same candidate ions from the more detailed model spectra presented by Blondin et al. (2015) for the Broad Line SN Ia 2002bo, yet additional investigations are needed to study the evolution of weak spectral signatures.

6.3.2 The 4110 Å feature

A similar set of conclusions follow when attempting to identify the 4110 Å feature, where both C II and Cr II have been proposed as the primary sources:

(i) Many events of varying peculiarities harbour a 4110 Å feature. This feature is blended for objects with either higher mean expansion velocities or a shallower decline in opacity along the line of sight. By contrast, this 4110 Å feature is resolved and therefore more conspicuous for objects with lower mean expansion velocities that just so happen to have conspicuous C II λ6580 absorption features, but not necessarily strong or detectable signatures of C II λ4267.

(ii) Despite a relatively strong and long-lasting C II λ6580 absorption feature, the increasingly conspicuous 4110 Å feature for SN 2007if and 2009dc disfavours the interpretation of a simultaneously prolonged detection of C II λ4267 for at least epochs nearest to maximum light and thereafter (Taubenberger et al. 2013).

(iii) In Fig. 10 we show that a deep and wide C II λ7234 absorption – as parametrized with high Boltzmann excitation temperatures in SYNAPPS – is not comparable with the observations during the relevant epochs. Furthermore, it is likely that species including S II, Cr II, and (PV + HV) Fe II also influence the shape and depth of the 4110 Å feature, and without invoking LTE excitation temperatures greater than 15 000 K (Scalzo et al. 2010; Taubenberger et al. 2013). Additionally, or at least for some Broad Lined SN Ia during the first 22 d post-explosion, the region near 4110 Å overlaps with weak signatures of S III λ4254 as well (Blondin et al. 2015); i.e. this for a subtype of SN Ia where high-ionization species such as S III are generally not considered for spectral decompositions.

(iv) A C II λ4267 absorption feature is not well-matched to the 4110 Å feature once the half-blended C II λ6580 line is centred near 13 000 km s^{-1}, nor at 12 000 km s^{-1}. If the 4110 Å feature were simply due to C II λ4267 alone, then it could be used to anchor v_{min} towards slightly lower values. However, we cannot rule in C II λ4267 as primarily responsible for the shape and evolution of the 4110 Å feature, and this is in agreement with notions previously expressed by Taubenberger et al. (2013).

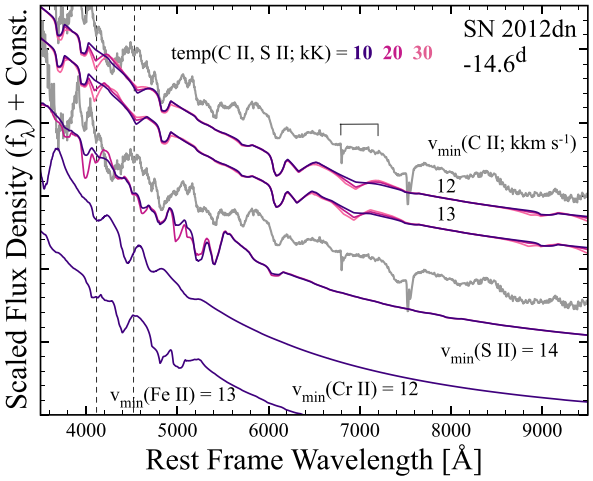

Figure 10. The day −14.6 spectrum of SN 2012dn, plotted twice in grey for clarity, is compared to a computed spectrum including Si II and C II, and single-ion calculations for S II, Cr II, and Fe II. Excitation temperatures (in units of Kelvin × 1000^{-1}) and expansion velocities (in units of km s^{-1} × 1000^{-1}) are varied for C II and S II as shown. Vertical dashed lines mark the locations of the 4100 Å and 4550 Å features.

6.4 C III λ4649

In the previous section we found C II is not particularly favoured as the primary contributor to the 4110 and 4550 Å features. However, the degeneracy of candidate ions for these weak features is manyfold, and simply in terms of unburned carbon.

For example, C I λλ4772, 4932may contribute to regions near 4550 Å. Considering the low-ionization potential of neutral carbon, one might expect minimal contribution from C I λλ4772, 4932. Therefore simultaneous optical+NIR data and detailed modelling would be needed to investigate further (Höflich et al. 2002; Hsiao et al. 2015; Marion et al. 2015).

In addition, the region between 4450 Å and 4550 Å in the day −14.6 spectrum of SN 2012dn could be influenced by C III λ4649 with a line velocity of ∼9600–13 000 km s^{-1}. Given a relatively weak 4550 Å signature, we did not include C III in the prescription of ions used for SN 2012dn in the previous sections. However, SYNAPPS would favour C III closer to v_{min} = 12 000 km s^{-1} (± 1000 km s^{-1}) given the consistency with values inferred from other species. Moreover, both C III and S III have similar ionization potentials, and this pairing has been suggested for SN Ia such as SN 1991T, 1997br, and 1999aa (Hatano et al. 2002; Garavini et al. 2004; Parrent et al. 2011).

In Fig. 11 we compare pre-maximum spectra of SN 1991T, 1997br, 1999aa, and 2012dn. We have also plotted the day −7 spectrum from the delayed-detonation series computed by Sasdelli et al. (2014) who concluded that the carbon-rich progenitor material in SN 1991T was burned out to ∼12 500 km s^{-1}, leaving no signatures of carbon (top of Fig. 11 in red). In Fig. 11 we also compare SN 1991T to a preliminary SYN++ spectrum. With v_{min} set to 11 500 km s^{-1} (± 1000 km s^{-1}) for each ion, the fit includes mostly Fe III, but also minor contributions from C III, Si II, Si III, S III, Fe II, Co III, and Ni II as these species do a fair job at reproducing most features.

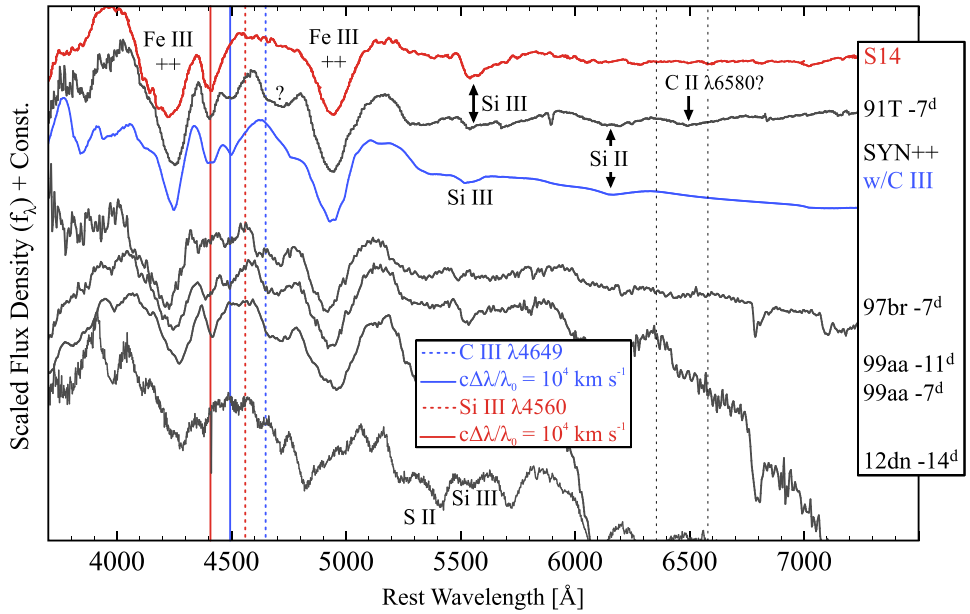

Figure 11. Comparisons between the delayed detonation spectrum from Sasdelli et al. (2014) (S14; day −7); our preliminary SYN++ spectrum with C III included in the full fit (see text of Section 6.4); and so-called 'Shallow Silicon', SN 1991T/1999aa-like SN Ia and SN 2012dn. Spectrum references: SN 1991T (Mazzali, Danziger & Turatto 1995); SN 1997br (Li et al. 1999); SN 1999aa (Garavini et al. 2004). The dotted, vertical lines are centred at 6355 Å and 6580 Å, and the 'Fe III++' signifies 'more than Fe III'.

As was previously discussed by Hatano et al. (2002), Garavini et al. (2004), and Parrent et al. (2011), there is a distinct feature near 4500 Å in the pre-maximum spectra of SN 1991T, 1997br, and 1999aa that could be significantly shaped, in part, by C III λ4649 forming near ∼11 500 km s^{-1}. Sasdelli et al. (2014) claim 'carbon lines are never detected' for SN 1991T in spite of the well-placed weak signature near 4500 Å, yet this feature is not reproduced in the computed spectra of Sasdelli et al. (2014) for an alternative interpretation.

This might imply that either the ionization balance for the model is inaccurate (possibly due to an assumed diffusive inner boundary; cf. Blondin et al. 2015), or too much carbon has been burned in the model. Without more advanced analysis of SN 1991T spectra from PHOENIX and CMFGEN, we therefore cannot rule out an identification of C III in these SN 1991T-like events.

Singly ionized species might also account for some of the more weaker features observed for SN 1991T-like events. For example, by day −7 for SN 1991T it is difficult to rule out weak contribution from Si II near 6150 Å. Notably, the computed spectrum of Sasdelli et al. (2014) shown in our Fig. 11 does not account for the 6150 Å feature until three days later (see their fig. 2).

A more fleeting identification for SN 1991T – one that would further support the tentative detection of C III λ4649 – is that of C II λ6580. Curiously, a weak depression redwards of 6300 Å is present in the day −11 spectrum of SN 1991T and for sometime thereafter.

In Fig. 12 we compare time series spectra of SN 2012dn and 1991T in terms of line velocities $\mathcal{O}$(v/c) of C II λλ6580, 7234 in order to access any common overlap between these two line signatures. This method was exploited by Parrent et al. (2011) for more normal SN Ia, where it was found to be a good indicator of detectable C II (see also Thomas et al. 2004). Therefore, while we attempt to take advantage of common overlap in the Doppler frame in Fig. 12, we also emphasize that first-order estimates of projected Doppler velocities are not accurate, much less for solitary weak depressions

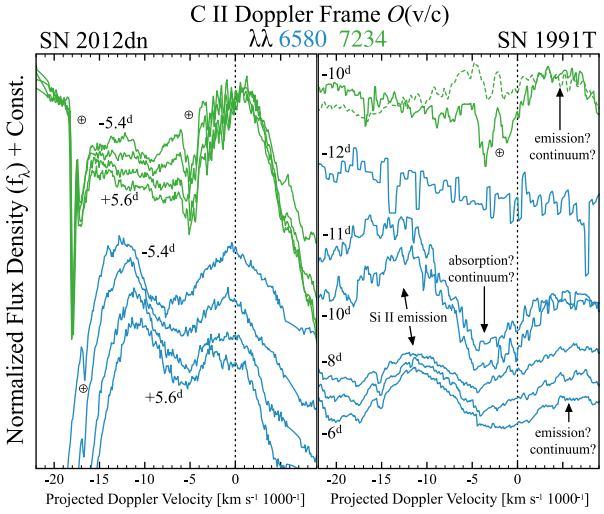

Figure 12. Time-series observations of SN 2012dn (this work) and 1991T (Mazzali et al. 1995) are compared in the Doppler frame $\mathcal{O}$(v/c) of C II λ6580 (blue) and λ7234 (green). In the right-hand panel, the day −10 spectra from Mazzali et al. (1995) (solid green) and Filippenko et al. (1992) (dashed-green) are used to inspect the 7000–7200 Å region of SN 1991T.

in the spectrum that may simply be continuum (cf. Branch 1977; Jeffery & Branch 1990).

From the available data on SN 1991T, invoking a detection of weak C II λλ6580, 7234 is troublesome. In particular, it is unclear where the would-be feature spanning 6350–6720 Å ends and where the continuum begins. Furthermore, bona fide absorption signatures of C II λ6580 in normal SN Ia are not often reported redwards of ∼6420 Å (Pereira et al. 2013).

By comparison, the bulk of the C II λ6580 signature in the day +5.6 spectrum of SN 2012dn extends to ∼6520 Å, with a flat component extending towards ∼6600 Å. However, absorption from a parent line of C II λ6580 is not thought to be physical beyond a rest-wavelength of 6580 Å during photospheric phases. Therefore, our best interpretation is that the flat component centred about 6580 Å is a result of either competing emission between C II and Si II, or an indication that some C II is confined to a blob or shell-like structure (see Jeffery & Branch 1990; Thomas et al. 2007).

As for SN 1991T, the feature nearest to 6580 Å is clearly too far redwards to be associated with C II by day −6. However, prior to day −7, what exactly is producing the minimum is unclear, yet the observations are not necessarily consistent with a non-detection of faint C II. In Fig. 12, the day −10 spectra of SN 1991T from Mazzali et al. (1995) (solid green) and Filippenko et al. (1992) (dashed-green) are also too noisy to search for a weaker signature of C II λ7234.

For SN 2012dn, where C II λ6580 is detected with a mean expansion velocity of ∼12 500 km s^{-1}, a weak 4450 Å feature that can be reasonably pinned to C III λ4649 at ∼12 500 km s^{-1} is only observed on day −14.6, and is therefore unconfirmed as a feature. Thus, while we cannot rule out contribution from C III near 4450 Å, it would appear that signatures from C III are minimal for SN 2012dn during photospheric phases.

7 DISCUSSION

If a companion star is necessary for the runaway explosion of SN Ia-like events (cf. Chiosi et al. 2015), its identity and role in the diversity of post-explosion spectra remain fairly ambiguous (Maeda, Kutsuna & Shigeyama 2014; Moll et al. 2014; Tanikawa et al. 2015). Additionally, there are many scenarios that may explain spectroscopic diversity as projections of distinct progenitor systems. Extreme events, e.g. SN 1991bg and 2002cx, may result from mechanisms or progenitor channels that are distinct from those most representative of the true norm of SN Ia (Hillebrandt et al. 2013 and references therein). A true norm could also originate from multiple binary configurations and explosive conditions (Benetti et al. 2005; Blondin et al. 2012; Dessart et al. 2014). Similarly, select subclasses may either represent bimodal characteristics of one or two dominant channels (Maeda et al. 2010; Maund et al. 2010; Röpke et al. 2012; Liu et al. 2015), or a predominant family where continuous differences such as progenitor metallicities (among other parameters) yield the observed diversity (Nugent et al. 1995; Lentz et al. 2000; Höflich et al. 2002; Maeda et al. 2014; Scalzo et al. 2014a). A dominant one (or two) progenitor system + explosion mechanism might then manifest properties about the norm that reach out into the same observational parameter space inhabited by the most peculiar subgroups (Baron 2014).

Nevertheless, an intriguing circumstance for SN Ia is that the evolution of spectral features, and possibly the spectroscopic make-up, of Core Normal events can be considered similar, as a whole, to those of SN 2006gz, 2009dc, and 2012dn. Perhaps this would not be surprising since both classes of SN Ia are expected to originate from WD progenitor systems. However, here we are referring to traceable similarities between Core Normal and SCC SN Ia in the context of the contrasting spectroscopic make-up compared to peculiar SN 1991T-like, 1991bg-like, and 2002cx-like events (Branch et al. 2004; Doull & Baron 2011; Parrent et al. 2011).[4]

7.1 Does a unique physical sequence exist between normal and SN 2012dn-like events?

If we assume that most normal SN Ia yield similar rise-times (∼19 d), near-maximum light expansion velocities (∼11 000 km s^{-1}), and opacities ($\kappa = 0.1$ cm^2 g^{-1}), the values assumed for SN 2012dn (v_{max} ∼11 000 km s^{-1}, t_{rise} ∼ 20 d; Chakradhari et al. 2014) indicate M_{ej}^{12dn} ∼ (90–120 per cent) × M_{Ch} = 1.3–1.7 M$_\odot$. 'By mass', SN 2012dn is not clearly SN 2009dc-like despite appearances (cf. Pinto & Eastman 2000a,b; Foley et al. 2009).[5] Furthermore, Chakradhari et al. (2014) used Arnett's rule (Arnett 1982) and $\log L_{bol}^{peak}$ = 43.27 erg s^{-1} to estimate that SN 2012dn produced 0.70–0.94 M$_\odot$ of ^{56}Ni. Assuming SN 2011fe and SN 2012dn have similar rise-times, Brown et al. (2014) estimated the mass of ^{56}Ni could be as low as ∼0.5 M$_\odot$, where part of the uncertainty is in the rise-time of SN 2012dn.[6] By comparison, the bolometric luminosity of SN 2011fe is consistent with the production of ∼0.42–0.64 M$_\odot$ of ^{56}Ni (Pereira et al. 2013), which is anywhere between half as much to slightly less than the amount of ^{56}Ni inferred for SN 2012dn.

For SN 2012dn, a significant fraction of the luminosity may be due to close circumbinary interaction with C+O-rich material. Therefore, the inferred mass of ^{56}Ni needed to reproduce the observed rise-time would be artificially higher (Taubenberger et al. 2013). Brown et al. (2014) also report that the integrated luminosities of SN 2011aa, 2012dn (two SCC SN Ia), and the normal and already NUV-blue SN 2011fe are quite similar despite the brighter UV luminosities for the SCC SN Ia (Milne & Brown 2012; Milne et al. 2013). Thus, it seems plausible that SN 2011fe and SN 2012dn could have produced comparable amounts of ^{56}Ni (± 0.10–0.20 M$_\odot$), where SN 2012dn obtained additional luminosity from close interaction ($\lesssim 10^9$ cm) with a larger exterior region of carbon-rich material.

Our estimates of v_{min} for C II, O I, Si II, and Ca II for SN 2011fe and 2012dn are shown in Fig. 13. Notably, SN 2006gz, 2009dc, 2011fe, and 2012dn show a similar overlap between O, Si, and Ca-rich material, while carbon-rich regions for SCC SN Ia share similar velocities found for Core Normal SN Ia as well (∼11 000–15 000 km s^{-1}). Compared to SN 2011fe, SN 2012dn only displays lower parametrized expansion velocities of PV Si II during the initial stages of homologous expansion; i.e. PV Si II in SN 2011fe falls

[4] For comparison among proposed spectral sequences of SN, a far more diverse set of events, i.e. those of type IIbIbc and IIPLn, separately, are sometimes viewed as also forming a physically related sequence of progenitor configurations (Nomoto et al. 1996; Claeys et al. 2011; Dessart et al. 2012; Smith et al. 2015, see also Maurer et al. 2010). For SN IIbIbc, one of the key questions is how many 'hydrogen-poor SN IIb' are misidentified as 'hydrogen-poor SN Ib' when both events are primarily discovered and typed during a 'type Ib' phase (Chevalier & Soderberg 2010; Arcavi et al. 2011; Milisavljevic et al. 2013; Folatelli et al. 2014; Parrent et al. 2015).

[5] If v_{max}^{12dn} = 11 000 ± 1500 km s^{-1}, v_{max}^{SNIa} = 12 000 ± 2500 km s^{-1}, t_{rise}^{12dn} = 20 ± 1.5 d, and t_{rise}^{SNIa} = 19.3 ± 0.5 d (Conley et al. 2006), then M_{ej}^{12dn} ∼ (70–130 per cent) × M_{Ch} = 1.0–1.8 M$_\odot$; the uncertainty is largely due to the poorly determined span of intrinsic mean expansion velocities. An additional uncertainty might arise from any difference between the mean opacities for normal and SN 2012dn-like events. See also Wheeler, Johnson & Clocchiatti (2015).

[6] Chakradhari et al. (2014) estimate a lower limit of 15.87 d.

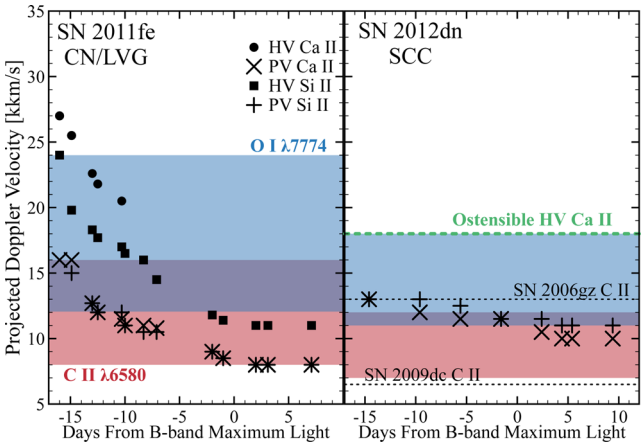

Figure 13. Initial SYNAPPS measurements and comparisons between the 'Core Normal', low-velocity gradient (CN/LVG) SN 2011fe and the SCC SN 2012dn. Symbols are defined in the left-hand panel. Red and blue colours denote the span of inferred line velocities for C II λ6580 and O I λ7774, respectively, and the purple shade indicates overlap between the two. Owing to spectroscopic blending of weak identifying signatures, estimates for C II and O I are given as broad ranges corresponding to C II λ6580 and O I λ7774, respectively, rather than more well-determined v_{min}(t).

below that of SN 2012dn shortly thereafter between day −10 and day −5.

For SN 2012dn, a non-detection of strong HV Ca II is obvious upon visual inspection of the 8200 Å feature. However, we cannot rule out a faint signature of trace HV Ca II at ∼19 000 km s^{-1} during pre-maximum epochs (Section 6.2). If a region of detached HV Ca II exists along the light-of-sight for SN 2012dn, then it is coincident with the lower extent of parametrized HV Ca II found in SN 2011fe (see Fig. 13).

Such considerations neither prove nor suggest that progenitor channels producing Core Normal and SCC SN Ia subtypes are remotely identical, and similarly among other SN Ia prototypes. Rather, they underscore the need for additional detailed investigations of spectroscopic degeneracies from single and double-degenerate scenarios (Röpke et al. 2012; Dan et al. 2015; Miles et al. 2015).

7.2 Differentiation through environmental properties

It may be possible to isolate candidate progenitor scenarios by noting the properties of the host-environment and host galaxy of a given event or SN Ia subclass (Hamuy et al. 1995; Hicken et al. 2009; Wang et al. 2013; Pan et al. 2014; Foley 2015; Maguire et al. 2015). The general finding has been that brighter, 'higher stretch SN Ia' tend to occur in metal-poorer environments of low-mass host galaxies (Sullivan et al. 2010; Childress et al. 2011; Khan et al. 2011), while sub-luminous, 'low-stretch SN Ia' are preferentially detected in environments indicative of an older (or delayed) population of progenitor systems (Howell 2001; Gallagher et al. 2008).

However, this assumes that each spectroscopic subtype identically follow the above mantra, per host-property, which may not be the case (Hicken et al. 2009). Specifically, the light-curve stretch of one particular progenitor class or SN Ia spectroscopic subtype, may tend to increase with metal-poor environments while another may not (Kobayashi & Nomoto 2009; Kistler et al. 2013). In turn, this could serve as a means for separating progenitor scenarios or a sequence of progenitor masses for one dominant progenitor family (Scalzo et al. 2014a,c). However, the extent of such an effect remains unclear given the difficulty of classifying events from sporadically sampled spectra.

Below we use empirical relations found in the literature to place crude estimates on the host-galaxy mass and local metallicity to compare SN 2012dn to so-called nearest neighbour SN Ia (Jeffery et al. 2007). We also inspect the percentages of SN Ia subclasses in the Palomar Transient Factory (PTF, Rau et al. 2009; Maguire et al. 2014) sample that was recently utilized by Pan et al. (2014, 2015) to investigate possible correlations between SN Ia light-curve stretch and local properties of the host environment.

7.2.1 *Estimation of host galaxy mass and metallicity*

SN 2012dn is located 35 arcsec west and 3 arcsec south of the purportedly normal spiral (SAcd) galaxy, ESO 462-16 (= PGC 64605; Bock et al. 2012), which belongs to a pair of binary galaxies (Soares et al. 1995). To estimate the host galaxy mass of SN 2012dn and hosts of other SN Ia (Section 6.2.2), we implement the empirical relation of Taylor et al. (2011):

$$\log \mathrm{M}/\mathrm{M}_{\odot} = 0.70(g-i) - 0.40M_{I,\mathrm{AB}} - 0.68 \quad (1)$$

and values obtained from NED and LEDA.[7]

Since our estimates here are not for precision cosmology, we assume representative errors by computing $\log M_{\mathrm{Stellar}} \equiv \log M/\mathrm{M}_{\odot}$ from equation (1) for the host of SN 2011fe, M101, and comparing to $\log M_{\mathrm{Stellar}} = 10.72^{+0.13}_{-0.12}$ obtained by van Dokkum, Abraham & Merritt (2014). Assuming $g-i$ = 1.0, $\mathrm{m}_{I,\mathrm{AB}} \sim 7.8\pm0.2$, DM = 29.1±0.2 ($H_0$ = 69.7 km s^{-1} Mpc^{-1}; Hinshaw et al. 2013) for M101, equation (1) yields $\log M_{\mathrm{Stellar}} \sim 8.6$. Following the same procedure for the host of SN 2012dn, and taking the above discrepancy for M101 as a conservative error estimate, we obtain a broad window (±2.2) for all points in Fig. 15 below; i.e. approximately two orders of magnitude too broad to draw association with a particular progenitor environment or scenario for the present study.

We estimate the metallicity of SN 2012dn's progenitor from optical spectroscopy of the host environment. The SN flux dominates the host galaxy emission lines at the precise location of the explosion site, so we instead extract spectra from three nearby H II regions which intersected our spectroscopic slit. To model the emission line spectra and measure the fluxes of the strong emission lines, we apply the Markov Chain Monte Carlo method of Sanders et al. (2012a). We then estimate metallicity using the N2 and O3N2 diagnostics of (Pettini & Pagel 2004; hereafter, PP04). Our spectra do not cover the [O II] λ3727 line, and we are therefore unable to estimate metallicity using diagnostics based on the R_{23} line ratio.[8]

We find metallicity values largely consistent between the three studied regions, ranging between $\log(\mathrm{O/H})_{\odot} + 12 = 8.4$–$8.6$, or ∼0.4−0.8Z$_{\odot}$ on the PP04 scale (Z$_{\odot} \equiv \log(\mathrm{O/H})_{\odot} + 12 = 8.69$; Asplund, Grevesse & Sauval 2005). The uncertainty in this estimate is small, ∼0.05 dex as estimated from propagation of the emission line flux uncertainties. In particular, we find $\log(\mathrm{O/H})_{\odot} + 12 = 8.48 \pm 0.06$ in the PP04N2 diagnostic for the region nearest to the explosion site. This uncertainty is likely to be dominated by systematic effects such as the calibration variance

[7] NED – http://ned.ipac.caltech.edu/; LEDA – http://leda.univ-lyon1.fr/. For M101, we assume log f_{ν} (Jy) ∼0.45 at λ ∼ 0.806 μm.

[8] $R_{23} \equiv$ ([O III] λ4959+5007] + [O II] λ3727])/Hβ (McGaugh 1991; Kewley & Dopita 2002).

Table 3. Metallicity estimates of literature SN Ia.

SN name	Approximate metallicity ($Z/Z_{\odot}$)	Reference number
2003fg	0.5	Khan et al. (2011)
2006gz	0.25	Khan et al. (2011)
2007if	0.15–0.20	Khan et al. (2011)
		Childress et al. (2011)
2009dc	0.38–0.52	Silverman et al. (2011)
2011fe	0.3–0.5	Mazzali et al. (2014)
2012dn	0.4–0.8	This work

in the strong line metallicity diagnostics, local metallicity variation in the host galaxy, and chemical evolution and host environment physical offset associated with the delay time between the birth and explosion of the progenitor star (Kewley & Ellison 2008; Sanders et al. 2012a,b, see also Pan et al. 2014; Soker 2014; Toonen, Voss & Knigge 2014).

On average, the metallicity inferred for the local environment of SN 2012dn places it at higher values relative to other SCC SN Ia (see Table 3). If these values were accurate enough for comparisons (cf. Niino, Nagamine & Zhang 2015), then at face value they would imply SN 2012dn originated from a progenitor with a metallicity no less than those giving rise to SN 2003fg, 2009dc, and the Core Normal SN 2011fe. However, it is only the metallicity estimate for SN 2011fe that stems from comparisons of UV spectra and abundance tomography (Mazzali et al. 2015; Baron et al. 2015). Thus, the context by which to properly estimate and interpret progenitor metallicities with certainty remains absent (Brown et al. 2015).

7.2.2 Bulk trends in SN Ia samples

Visual classification of SN spectra is sometimes described as a subjective or ambiguous process, whereby a computer is needed to facilitate the problem (Sasdelli et al. 2015).[9] Between normal and peculiar events, or events within one subclass, this is somewhat true for noisy, post-maximum phase spectra, i.e. when spectroscopic diversity declines between most SN Ia subtypes (Branch, Dang & Baron 2009, and references therein). However, the unambiguous patterns established by pre-maximum light data indicate sub-classification can be done by-eye when the event is caught early enough and followed up by campaigns of high-quality observations. This is because noticeable differences of both major and minor features are often related to respective differences in the composition of the outermost regions of ejecta (Tanaka et al. 2008).

With today's large spectrum-limited data sets, a computer is indeed ideal for charting dissimilarities between events in a given subclass, such as homogeneous Core Normal events most similar to SN 2011fe. This assumes, however, that some of the underobserved events in either a given sample or pre-defined subclass are not caught-late or 'peculiar' outliers for a neighbouring, and possibly unrelated, subclass such as Broad Line SN Ia (see also Folatelli et al. 2014; Parrent et al. 2015). In fact, there is curious overlap between events that have been typed as 'high velocity Core Normal' and 'normal velocity Broad Line' SN Ia (Blondin et al. 2012; Parrent 2014). Therefore, the vetting process for these and other subclasses of type I supernovae would benefit from spectral decomposition through Gaussian processes (Fakhouri et al. 2015) and machine learning methods (Sasdelli et al. 2015).

From a sample of 82 PTF SN Ia, Pan et al. (2014) conducted a follow-up investigation of empirical relationships between SN Ia light-curve stretch and various properties of the host environment, including host galaxy mass, specific star formation rates, and gas-phase metallicities. Previous conclusions were reached insofar as the stellar mass of the host is correlated in the light-curve shape of the subsequent explosion (Sullivan et al. 2010; Kim et al. 2014). However, as with most previous surveys of SN Ia host-environments, visual details on the spectroscopic diversity of this most recent sample were omitted (see later Pan et al. 2015).

In terms of signal-to-noise ratios and spectroscopic follow-up, it is important to note the data of the 82 PTF SN Ia are of low to moderate quality. Similar to spectra obtained by the SuperNova Legacy Survey, PTF SN come with a few sporadically sampled optical spectra on average. As sub-classifications of supernovae are more accurately determined by time series data sets, a lack of coverage inhibits a precise recording of those defining features most often associated with spectroscopic peculiarity, particularly during pre-maximum phases. For a visualization of this, Parrent et al. (2014) presented a follow-up efficiency diagram in their fig. 4. The PTF sample was included in this diagram, falling towards the bottom-left corner of their figure inset.

Since we cannot attempt a consistent quantification of known subtypes for the PTF sample, our assessments here, and similarly for the study of high-velocity features by Pan et al. (2015), are based on visual comparisons to time series observations of SN Ia that have been designated as 'well-observed' throughout the literature. Several examples of our by-eye sub-classifications are detailed in Fig. 14.

To illustrate the distribution of SN Ia subtypes for a given SN sample, we focus on the light-curve stretch versus $\log M_{\rm Stellar}$ plane (see fig. 9 of Pan et al. 2014). In Fig. 15 we have replotted the PTF sample as grey + symbols. The colours per subtype are in reference to the classification criteria of Branch et al. (2006); filled black circles for Core Normal, green for Broad Line, red for Shallow Silicon, blue for Cool, and purple for super-Chandrasekhar mass candidate events. For PTF SN Ia that appear normal but are suspected as having properties of neighbouring subtypes, e.g. Core Normal, Broad Line, and a selection of peculiar hybrids such as SN 1999aa, we have marked these as coloured open circles where appropriate, and we consider this as an error estimate below. Objects for which a spectroscopic subtype could not be determined from an appropriate time series data set are marked as grey ×s. A number of these cases are related to an inability to disentangle normal velocity SN 1984A-like from high[er] velocity SN 1994D-like events, even after enforcing an artificial selection criterion such as a maximum light separation velocity of 11 800 km s^{-1} (Wang et al. 2009b) or 12 200 km s^{-1} (Blondin et al. 2012).

In Table 4 we list estimates of SN Ia subtype percentages for the sample in terms of `SiFTO` light-curve stretch and find considerable room for additional trends, per subtype. Here, the overall trend between $\log M_{\rm Stellar}$ and light-curve stretch is built from a heterogenous aggregate of visibly distinct SN Ia, with traceable peculiarities, that may or may not be physically related to other spectroscopic subtypes included in the sample. As such, the claim of 'higher stretch SN Ia originate from low-mass, metal-poor environments' is not explicitly with regards to Core Normal, SN 2011fe-like SN Ia with light-curve stretch values between 0.8 and 1.3 (see Fig. 15). Pan

[9] This problem is not unique to supernova spectra. Solar spectroscopists, among others, have faced a similar debate, and we refer the reader to p. 23 of 'Stellar Spectral Classification' (Gray & Corbally 2009) and Keenan (1984) where visual classification of stellar spectra is discussed.

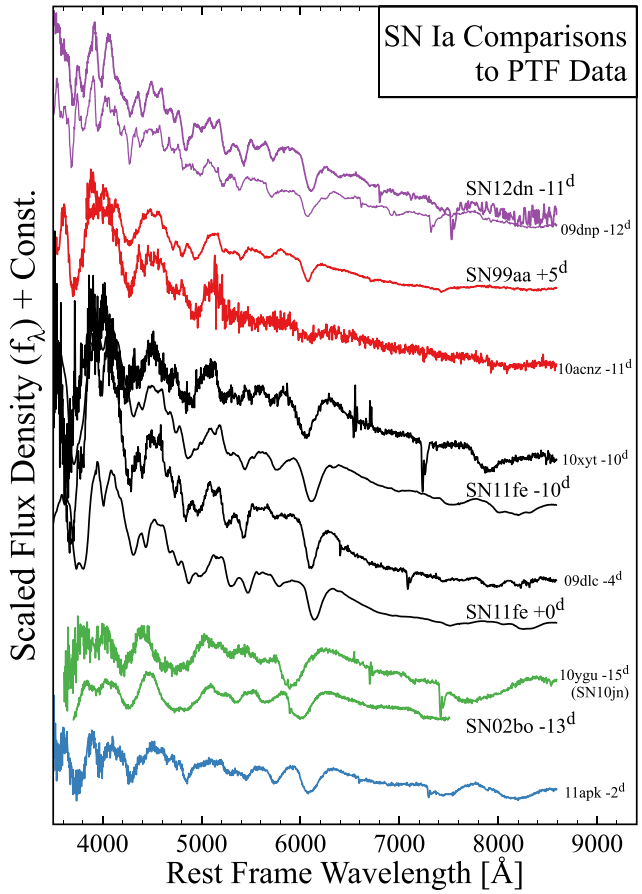

Figure 14. Comparisons between literature SN Ia, SN 2012dn, and some of the best-observed PTF SN Ia discussed in Pan et al. (2014, 2015). The colours per subtype are in reference to the classification criteria of Branch et al. (2006); filled black circles for Core Normal, green for Broad Line, red for Shallow Silicon, blue for Cool, and purple for super-M_{Ch} mass candidate events.

et al. (2014) do not claim otherwise; however, we find it important to explicitly show these details when addressing bulk trends pertaining to, e.g. properties of the host.

The percentages of each subtype in the PTF sample are also distinct from those found in the volume-limited sample of Li et al. (2011), where SN Ia were classified by likeness to a few historical prototypes (cf. Filippenko 1997 and fig. 13 of Doull & Baron 2011). We suspect a quantitative re-evaluation of SN Ia subtypes would better elucidate the multitude of trends involving SN Ia rates and host-galaxy properties.

7.2.3 Correlations with Ca II at high velocities

Pan et al. (2015) later analysed properties of Si II λ6355 and the Ca II near-infrared triplet profiles for 122 SN Ia and found trends relating to the stellar mass and star formation rates of the host galaxy. In particular, Pan et al. (2015) recover a trend, previously found by Maguire et al. (2012, 2014) and Childress et al. (2014), where maximum light spectra that have strong signatures of HV Ca II tend to also have broader light curves. All of these works deduce the relative strengths and velocities (weighted by the blended absorption minimum) of high-velocity features near maximum light using up to five Gaussian absorption profiles to encompass 11 P Cygni-like

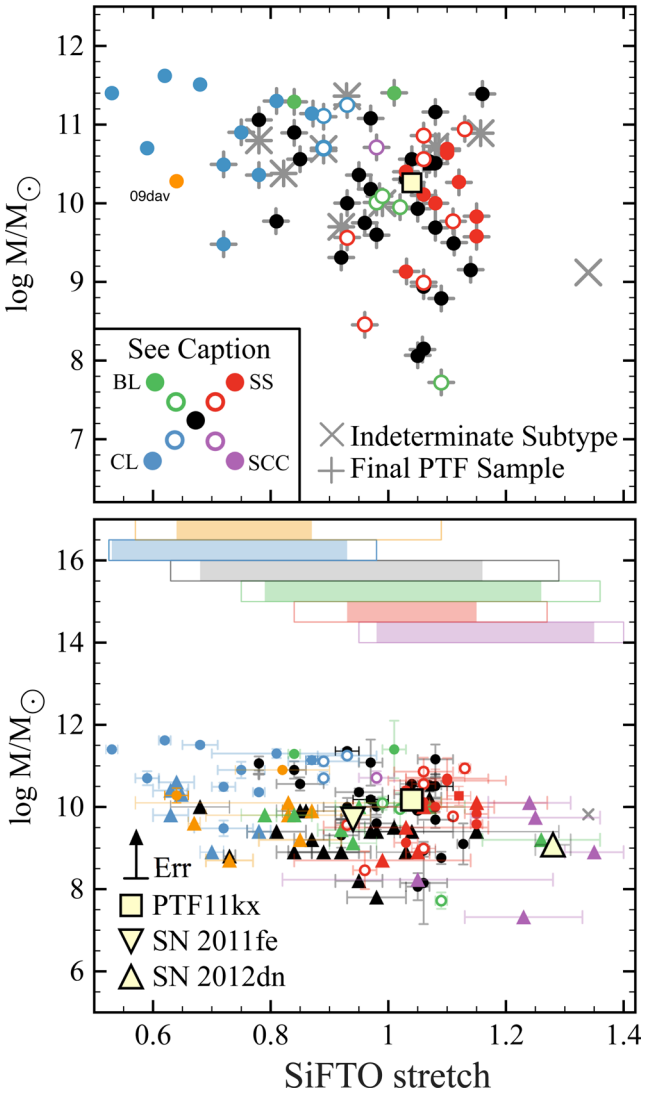

Figure 15. [Top] host galaxy mass versus light-curve stretch using the PTF sample SN Ia initially presented by Pan et al. (2014), shown as grey + symbols. Overplotted in colour are our best comparative guesses for the subtypes of each PTF SN shown. Colours are the same as in the adjacent legend, while orange circles denote Ia-peculiar events like SN 2002cx and PTF09dav. Open-circles indicate shared tendencies with a particular subtype. Grey ×s represent events with follow-up spectra too noisy or too late in epoch to visibly decipher a subtype. [Bottom] the above inset figure supplemented with literature SN Ia and estimates for host galaxy mass using the empirical relation of Taylor et al. (2011). Horizontal bars represent the span of light-curve stretch for each spectroscopic subtype shown. Here we are primarily concerned with the light-curve stretch axis. However, for the purposes of plotting all literature SN Ia, the triangles represent lower limit estimates of host galaxy mass as derived from equation (1) and normalized to that for M101. Errors for PTF objects are retained from Pan et al. (2014). [Note] In a previous version of Parrent (2014), the value for SN 2012dn's stretch in the plot did not match the correct value in Section 3 of this work.

lines; i.e. effectively narrow-band pass-filters with one Gaussian for PV Si II λ6355 and four gaussians for PV and HV Ca II to represent two unconstrained components of H&K and the infrared-triplet.

During pre-maximum epochs, such methods can break down without the inclusion of either parametrized HV Si II, or an extended region of Si II in absorption (cf. Blondin et al. 2015). Furthermore, it is not often that signatures of detached HV Si II are as prominently

Table 4. Estimates for SN Ia subtype contamination in the 'Quality Cut Sample' from Pan et al. (2014).

SN Ia subtype	Sample percentage	SiFTO stretch
Core Normal, SN 1994D, 2011fe, 2014J-likes	38−58 per cent	$0.78 < s < 1.16$
Broad Line; SN 1984A-, 2002bo-likes	3−9 per cent	$0.84 < s < 1.09$
Shallow Silicon, SN 1991T and intermediary 1999aa-likes	14−24 per cent	$0.93 < s < 1.15$
Cool, SN 1991bg and intermediary 2004eo-likes	9−13 per cent	$0.72 < s < 0.93$
Ia-CSM (PTF11kx) and super-Chandrasekhar candidate (PTF09dnp)	3 per cent	$s = 1.04$ and 0.98, respectively

observed as in the case of the peculiar SN 2012fr (Childress et al. 2013), nor does an interpretation of distinctly detached shells of HV Si II and HV Ca II necessarily follow quantitative consistency between observations and a prescription of PV + HV Si II and Ca II (Baron et al. 2015).

Additionally, parametrized HV components of Si II and Ca II inferred for the normal SN Ia 2011fe are not coincident in such a way that one can readily deduce the outermost extent of Ca II from that of Si II (see our Fig. 13). Moreover, the estimated expansion velocities for a detached component of HV Ca II can be uncertain by 2000–8000 km s^{-1} depending on the width of the feature and the observational coverage (see fig. 3 of Parrent 2014). There has also been evidence for multiple shells of high-velocity Ca II, as suggested for SN 2000cx (Thomas et al. 2004, see also Silverman et al. 2013).

Weak signatures of C I, O I, Mg II, and Fe II might also influence wavelengths that undergo absorption from the Ca II infrared-triplet. For events where there are sufficiently early pre-maximum spectra, e.g. SN 1994D and 2011fe, signatures of HV O I may be present as well (Branch et al. 2005; Nugent et al. 2011; Parrent et al. 2012). Near maximum light, one might also expect increased absorption from O I for fast-decliners such as SN 1991bg, 1997cn, 1999by, 2000dk, 2005bl, and 2007fr (Doull & Baron 2011 and references therein). More significant contributions may come from lines of Co II (Blondin et al. 2015). This translates to possibly overestimating contributions from parametrized PV Ca II and underestimating the extent of trace Ca II at relatively higher velocities, which can go unconfirmed without observations prior to ∼day −7.

Silverman et al. (2015) recently improved upon the methods of Maguire et al. (2012, 2014), Childress et al. (2014), and Pan et al. (2015) by considering *gf*-weighted line-strengths. Silverman et al. (2015) also test their method by fitting 11 out of 445 spectra with SYNAPPS. Some of their preliminary fits include PV components of O I, Mg II, Si II, Si III, S II, Ti II, Fe II, Fe III, and an additional HV component of Ca II.

Using SYNAPPS in this manner can effectively confirm the need for parameterizing HV Si II and HV Ca II; however, it does not support an accurate determination of parametrized velocities from Gaussian fitting methods where fewer ions are incorporated. This is primarily because the broad features of supernova spectra enable a gross approximation of semi-empirical quantities, which are dependent on optical-depth effects and ionization gradients in the outermost regions of ejecta.

On this point, the six fits shown in fig. 1 of Silverman et al. (2015), and particularly for SN 1994D, 2002dj, and 2012fr, indicate either an over/undershooting of velocities, or overly saturated lines. Silverman et al. (2015) do in fact attribute some of the discrepancies in their fits to the degeneracy between SYNAPPS parameters, $v_{\mathrm{min},\,Y}$ and logtau. Although, Silverman et al. (2015) do not show the simultaneous fit to the H&K and infrared-triplet region for any event (see also fig. 1 of Ben-Ami et al. 2015 and fig. 17 of Pignata et al. 2011), which is important for zeroing-in on self-consistent estimates of $v_{\mathrm{min},\,Y}$. Moreover, degeneracies between SYNAPPS parameters can be broken from time series fitting, and can also result in an improved time-dependent (and model-dependent) accuracy of a supposed separation velocity.

Still, studies that have attempted a complete tracing of SN Ia spectral features with SYNAPPS do not unanimously produce estimates of v_{min} better than $\sim\pm1000$ km s^{-1} (Parrent et al. 2012; Parrent 2014; and this work). Overall, the direct analysis methods of Parrent et al. (2012), Maguire et al. (2012, 2014), Childress et al. (2014), Pan et al. (2015), and Silverman et al. (2015) are so far unable to determine when a broad feature is due to a detached (and blended) component at higher velocities, and when the width of that feature is produced by a changing ionization gradient. These methods do give credence to the inclusion of parametrized HV components, but the inferred separation velocities remain uncertain outside of events similar to SN 2012fr.

Near maximum light, it is true that most events no longer harbour a strong feature near 8000 Å, or at least not similar to those of SN 1999ee, 2001el, and 2004S (which do not appear to have been included in the studies done by Childress et al. 2014 and Silverman et al. 2015). However, the inclusion of Broad Line events in the sample of Childress et al. (2014), such as SN 2006X, is debatable considering that line velocities for the Ca II infrared-triplet in SN 2006X overlap those of HV Ca II in some normal SN Ia (16 000–25 000 km s^{-1}), yet some have interpreted SN 2006X as having no high-velocity features because there are no distinguishable signatures of HV Ca II upwards of 20 000–30 000 km s^{-1} prior to maximum light (see also Silverman et al. 2015).

For SN Ia that exhibit spectral features of high-ionization lines, e.g. SN 1991T, 1998es, and 1999aa, the bulk of their infrared Ca II feature appears to peak in strength ∼1-week after maximum light. This is still consistent with a lack of strong signatures of HV Ca II near maximum light, yet Silverman et al. (2015) find favourable evidence for weak absorption from Si II and Ca II at nominally high velocities for some of these Shallow-Silicon events.

From a sample of 18 SN 1991bg-like events with coverage near maximum light, Silverman et al. (2015) conclude models of SN 1991bg should never produce high-velocity signatures. However, this too remains uncertain given that the only SN 1991bg-like event with a spectrum taken as early as day −6 is SN 2005bl (Taubenberger et al. 2008; Hachinger et al. 2009), and the normal SN Ia 2011fe effectively lost conspicuous signatures of highly blueshifted absorption in Ca II near day −10.

As for the positive correlation between the strength of HV Ca II near maximum light and the width of the light curve, there are SN Ia with broad light curves that do not also have strong, high-velocity features of Ca II, e.g. SN 2006gz, 2007if, and 2009dc (Silverman et al. 2015 and references therein). Yet from our analysis of SN 2012dn, we are still unable to directly rule out faint signatures of detached Ca II from its spectra using the relatively stronger H&K lines superimposed with Si II λ3858. Whether such a detection is physically realizable underscores the need for refining parameter ranges for SYNAPPS-like tools by calibrating to spectrum

synthesizers that incorporate an approximated abundance model, e.g. TARDIS (Kerzendorf & Sim 2014).

8 CONCLUSIONS

The time series spectra we obtained of SN 2012dn during its first month showed an evolution most similar to SCC SN Ia, but not as luminous as one might expect (Brown et al. 2014; Chakradhari et al. 2014). In particular, the weaker than normal signatures of Si II and Ca II, a stronger than normal signature of C II λ6580, and relatively slowly evolving line-velocities indicate that SN 2012dn is most closely associated with the SCC class of SN Ia. Late-time comparisons to SCC SN Ia also support an association between this particular subclass and SN 2012dn (see Chakradhari et al. 2014 and our Fig. 4).

The 11-component prescription of ions utilized here for deconstructing the photospheric phase spectra of SN 2012dn (Figs 5–10) afforded us an ability to provide internally consistent inferences of multiple line-velocities (Fig. 13), and can be improved upon (Parrent 2014). Compared to signatures of C II observed for the normal SN 2011fe, for SN 2012dn we estimate the material associated with C II is only $\sim$2000 km s^{-1} slower. As was similarly proposed for SN 2006bt (Foley et al. 2010b), Chakradhari et al. (2014) find the discordant velocity estimates of C II and Si II may indicate that the carbon-rich material is clumpy and off-centre from the line of sight. Whether or not this is the case awaits a larger sample of SN 2012dn-like events. Additionally, and unlike other so-called Shallow Silicon events such as SN 1991T, 1997br, and 1999aa, we find little evidence favouring a detection of C III λ4649 in the early phase spectra of SN 2012dn.

An important take away point from our analysis of SN 2012dn spectra in Section 6 and visual classification of PTF SN Ia in Section 7 is that a majority of SN spectral features are not caused by some underlying stochastic variation. Rather, signatures of atomic species form a highly blended spectrum that nature is frequently capable of reproducing, such that we have a few distinct SN Ia subtypes and a number of outliers that suggest a continuum. Yet a cross examination of spectra computed for super-$M_{\rm Ch}$ merging WDs (e.g. Pakmor et al. 2012; Moll et al. 2014; Raskin et al. 2014) reveals that, while these spectra resemble SN Ia-like events, they are not well-matched to observations of super-$M_{\rm Ch}$ candidates SN 2006gz and 2012dn, nor have they been shown to consistently predict the spectroscopic evolution of more normal SN Ia.

Namely, Moll et al. (2014) and Raskin et al. (2014) find line velocities that are too high for both normal SN Ia and events similar to SN 2012dn (upwards of 20 000 km s^{-1} near maximum light, and depending on the viewing-angle). Similarly, the maximum-light spectrum for the violent merger provided by Pakmor et al. (2012) has the appearance of predicting signatures of iron that are too strong compared to normal SN Ia, whereas signatures of intermediate-mass elements do not appear strong enough. Given that signatures of iron-peak and intermediate-mass elements in SN 2006gz and 2012dn are somewhat weaker than normal, and therefore weaker than some of the latest predictions of merging WDs, we are therefore unable to relate these progenitor scenarios in their current form to SN 2012dn.

In an attempt to differentiate a progenitor channel through other means, in Section 7 we examined the PTF sample used by Pan et al. (2014) who studied correlations between properties of the host galaxy and light-curve parameters of 82 SN Ia. However, in Section 7.2.2 we found that empirical measures such as light-curve width, or stretch, do not encompass the spectroscopic details for a given sample of SN Ia (see Figs 14 and 15), nor has the negative correlation between light-curve stretch and host-galaxy mass been shown to apply to all types of peculiar and more normal SN Ia within a given sample.

Current models of both single-degenerate delayed detonations (Kasen & Plewa 2007) and select WD mergers (Pakmor et al. 2012; Raskin et al. 2014; Dan et al. 2015) may account for multiple SN Ia subtypes as the distribution of ejected material is found to be asymmetric in some instances. Therefore, to investigate and clarify the relationships between spectroscopic diversity, properties of the host environment, and lifetimes of the progenitors, photometrically based SN surveys would benefit from enhanced spectroscopic monitoring of nearby supernovae, including events at redshifts greater than unity.

ACKNOWLEDGEMENTS

This work was supported by the Las Cumbres Observatory Global Telescope Network. This research used resources of the National Energy Research Scientific Computing Center, which is supported by the Office of Science of the US Department of Energy under Contract No. DE-AC02-05CH11231, and a grant from the National Science Foundation: AST-1211196. JV is supported by Hungarian OTKA Grant NN 107637.

We are indebted to Asa Bluck, Ruben Diaz, Peter Pessev, Kathy Roth, and Ricardo Schiavon for their critical role in obtaining the Gemini Target-of-Opportunity data with both Gemini facilities (PI, D. A. Howell, GN-2012A-Q-34 and GS-2012A-Q-20; processed using the Gemini IRAF package), which are operated by the Association of Universities for Research in Astronomy, Inc., under a cooperative agreement with the NSF on behalf of the Gemini partnership: the National Science Foundation (USA), the National Research Council (Canada), CONICYT (Chile), the Australian Research Council (Australia), Ministério da Ciência, Tecnologia e Inovação (Brazil) and Ministerio de Ciencia, Tecnología e Innovación Productiva (Argentina). Observations reported here were also obtained at the MMT Observatory, a joint facility of the Smithsonian Institution and the University of Arizona. Additional observations reported in this paper were obtained with the Southern African Large Telescope.

This work was also made possible from contributions to the SuSupect (Richardson et al. 2001) and WISeREP data bases (Yaron & Gal-Yam 2012), as well as David Bishop's Latest Supernovae page (Gal-Yam et al. 2013), and has made use of PTF data obtained and reduced by J. Cooke, S. Ben-Ami, and R. S. Ellis. JTP wishes to thank D. Branch, E. Baron, and A. Soderberg for helpful discussions and comments on previous drafts.

Finally, we wish to thank our anonymous referee for helpful comments on an earlier draft.

Facilities: Las Cumbres Global Telescope Network, Inc., Gemini, FTS, FLWO, SALT, MMT.

REFERENCES

Aldering G. et al., 2006, ApJ, 650, 510
Anderson J. P. et al., 2014, MNRAS, 441, 671
Anupama G. C., Sahu D. K., Deng J., Nomoto K., Tominaga N., Tanaka M., Mazzali P. A., Prabhu T. P., 2005, ApJ, 631, L125
Arcavi I. et al., 2011, ApJ, 742, L18
Arnett W. D., 1982, ApJ, 253, 785
Asplund M., Grevesse N., Sauval A. J., 2005, in Barnes T. G., III, Bash F. N., eds, ASP Conf. Ser. Vol. 336, Cosmic Abundances as Records of Stellar Evolution and Nucleosynthesis. Astron. Soc. Pac., San Francisco, p. 319
Baron E., 2014, Nucl. Phys. A, 928, 319

Baron E., Hauschildt P. H., Branch D., Wagner R. M., Austin S. J., Filippenko A. V., Matheson T., 1993, ApJ, 416, L21
Baron E., Hauschildt P. H., Nugent P., Branch D., 1996, MNRAS, 283, 297
Baron E. et al., 2015, MNRAS, 454, 2549
Ben-Ami S. et al., 2015, ApJ, 803, 40
Benetti S. et al., 2004, MNRAS, 348, 261
Benetti S. et al., 2005, ApJ, 623, 1011
Blondin S. et al., 2012, AJ, 143, 126
Blondin S., Dessart L., Hillier D. J., Khokhlov A. M., 2013, MNRAS, 429, 2127
Blondin S., Dessart L., Hillier D. J., 2015, MNRAS, 448, 2766
Bock G., Parrent J. T., Howell D. A., 2012, Cent. Bur. Electron. Telegrams, 3174, 1
Bongard S., Baron E., Smadja G., Branch D., Hauschildt P. H., 2006, ApJ, 647, 513
Bongard S., Baron E., Smadja G., Branch D., Hauschildt P. H., 2008, ApJ, 687, 456
Branch D., 1977, MNRAS, 179, 401
Branch D., Patchett B., 1973, MNRAS, 161, 71
Branch D., Baron E., Thomas R. C., Kasen D., Li W., Filippenko A. V., 2004, PASP, 116, 903
Branch D., Baron E., Hall N., Melakayil M., Parrent J., 2005, PASP, 117, 545
Branch D. et al., 2006, PASP, 118, 560
Branch D., Parrent J., Troxel M. A., Casebeer D., Jeffery D. J., Baron E., Ketchum W., Hall N., 2007, in di Salvo T., Israel G. L., Piersant L., Burderi L., Matt G., Tornambe A., Menna M. T., eds, Am. Inst. Phys. Conf. Ser., Vol. 924, The Multicolored Landscape of Compact Objects and Their Explosive Origins. Am. Inst. Phys., Sicily, Italy, p. 342
Branch D., Dang L. C., Baron E., 2009, PASP, 121, 238
Bravo E., García-Senz D., Cabezón R. M., Domínguez I., 2009, ApJ, 695, 1257
Brown P. J. et al., 2009, AJ, 137, 4517
Brown P. J. et al., 2010, ApJ, 721, 1608
Brown P. J. et al., 2012, ApJ, 753, 22
Brown T. M. et al., 2013, PASP, 125, 1031
Brown P. J. et al., 2014, ApJ, 787, 29
Brown P. J., Baron E., Milne P., Roming P. W. A., Wang L., 2015, ApJ, 809, 37
Burgh E. B., Nordsieck K. H., Kobulnicky H. A., Williams T. B., O'Donoghue D., Smith M. P., Percival J. W., 2003, in Iye M., Moorwood A. F. M., eds, Proc. SPIE Conf. Ser. Vol. 4841, Instrument Design and Performance for Optical/Infrared Ground-based Telescopes. SPIE, Bellingham, p. 1463
Chakradhari N. K., Sahu D. K., Srivastav S., Anupama G. C., 2014, MNRAS, 443, 1663
Chen M. C., Herwig F., Denissenkov P. A., Paxton B., 2014, MNRAS, 440, 1274
Chevalier R. A., Soderberg A. M., 2010, ApJ, 711, L40
Childress M. et al., 2011, ApJ, 733, 3
Childress M. J. et al., 2013, ApJ, 770, 29
Childress M. J., Filippenko A. V., Ganeshalingam M., Schmidt B. P., 2014, MNRAS, 437, 338
Childress M. J. et al., 2015, MNRAS, 454, 3816
Chiosi E., Chiosi C., Trevisan P., Piovan L., Orio M., 2015, MNRAS, 448, 2100
Cikota A., Deustua S., Marleau F., 2016, preprint (arXiv:1601.05659)
Claeys J. S. W., de Mink S. E., Pols O. R., Eldridge J. J., Baes M., 2011, A&A, 528, A131
Conley A. et al., 2006, AJ, 132, 1707
Conley A. et al., 2008, ApJ, 681, 482
Contardo G., Leibundgut B., Vacca W. D., 2000, A&A, 359, 876
Dan M., Guillochon J., Brüggen M., Ramirez-Ruiz E., Rosswog S., 2015, MNRAS, 454, 4411
Dessart L., Hillier D. J., Li C., Woosley S., 2012, MNRAS, 424, 2139
Dessart L., Blondin S., Hillier D. J., Khokhlov A., 2014, MNRAS, 441, 532
Dilday B. et al., 2012, Science, 337, 942
Doull B. A., Baron E., 2011, PASP, 123, 765
Fabricant D. G., Hertz E. N., Szentgyorgyi A. H., Fata R. G., Roll J. B., Zajac J. M., 1998, in D'Odorico S., ed., Proc. SPIE Conf. Ser. Vol. 3355, Optical Astronomical Instrumentation. SPIE, Bellingham, p. 285
Fakhouri H. K. et al., 2015, ApJ, 815, 58
Filippenko A. V., 1997, ARA&A, 35, 309
Filippenko A. V. et al., 1992, ApJ, 384, L15
Fisher A. K., 2000, PhD thesis, The University of Oklahoma
Fisher A., Branch D., Nugent P., Baron E., 1997, ApJ, 481, L89
Folatelli G. et al., 2014, ApJ, 792, 7
Foley R. J., 2013, MNRAS, 435, 273
Foley R. J., 2015, MNRAS, 452, 2463
Foley R. J. et al., 2009, AJ, 138, 376
Foley R. J., Brown P. J., Rest A., Challis P. J., Kirshner R. P., Wood-Vasey W. M., 2010a, ApJ, 708, L61
Foley R. J., Narayan G., Challis P. J., Filippenko A. V., Kirshner R. P., Silverman J. M., Steele T. N., 2010b, ApJ, 708, 1748
Foley R. J. et al., 2014a, MNRAS, 443, 2887
Foley R. J., McCully C., Jha S. W., Bildsten L., Fong W.-f., Narayan G., Rest A., Stritzinger M. D., 2014b, ApJ, 792, 29
Friesen B., Baron E., Branch D., Chen B., Parrent J. T., Thomas R. C., 2012, ApJS, 203, 12
Friesen B., Baron E., Wisniewski J. P., Parrent J. T., Thomas R. C., Miller T. R., Marion G. H., 2014, ApJ, 792, 120
Gal-Yam A., Mazzali P. A., Manulis I., Bishop D., 2013, PASP, 125, 749
Gallagher J. S., Garnavich P. M., Caldwell N., Kirshner R. P., Jha S. W., Li W., Ganeshalingam M., Filippenko A. V., 2008, ApJ, 685, 752
Garavini G. et al., 2004, AJ, 128, 387
Garavini G. et al., 2005, AJ, 130, 2278
Graham M. L. et al., 2014, ApJ, 787, 163
Gray R. O., Corbally J. C., 2009, Stellar Spectral Classification. Princeton Univ. Press, NJ
Guy J. et al., 2007, A&A, 466, 11
Guy J. et al., 2010, A&A, 523, A7
Hachinger S., Mazzali P. A., Taubenberger S., Pakmor R., Hillebrandt W., 2009, MNRAS, 399, 1238
Hachinger S., Mazzali P. A., Taubenberger S., Fink M., Pakmor R., Hillebrandt W., Seitenzahl I. R., 2012, MNRAS, 427, 2057
Hachinger S. et al., 2013, MNRAS, 429, 2228
Hachisu I., Kato M., Saio H., Nomoto K., 2012, ApJ, 744, 69
Hamuy M., Phillips M. M., Maza J., Suntzeff N. B., Schommer R. A., Aviles R., 1995, AJ, 109, 1
Hatano K., Branch D., Fisher A., Millard J., Baron E., 1999a, ApJS, 121, 233
Hatano K., Branch D., Fisher A., Baron E., Filippenko A. V., 1999b, ApJ, 525, 881
Hatano K., Branch D., Qiu Y. L., Baron E., Thielemann F., Fisher A., 2002, New Astron., 7, 441
Hershkowitz S., Wagoner R. V., 1987, ApJ, 322, 967
Hershkowitz S., Linder E., Wagoner R. V., 1986a, ApJ, 301, 220
Hershkowitz S., Linder E., Wagoner R. V., 1986b, ApJ, 303, 800
Hicken M., Garnavich P. M., Prieto J. L., Blondin S., DePoy D. L., Kirshner R. P., Parrent J., 2007, ApJ, 669, L17
Hicken M. et al., 2009, ApJ, 700, 331
Hillebrandt W., Kromer M., Röpke F. K., Ruiter A. J., 2013, Frontiers Phys., 8, 116
Hinshaw G. et al., 2013, ApJS, 208, 19
Höflich P., Gerardy C. L., Fesen R. A., Sakai S., 2002, ApJ, 568, 791
Hook I. M., Jørgensen I., Allington-Smith J. R., Davies R. L., Metcalfe N., Murowinski R. G., Crampton D., 2004, PASP, 116, 425
Howell D. A., 2001, ApJ, 554, L193
Howell D. A. et al., 2006, Nature, 443, 308
Howell D. A., Sullivan M., Parrent J., Nugent P., Hook I., Dilday B., Maguire K., Graham M., 2012, Early-time observations of Type Ia supernovae to reveal progenitors. GEM-N, NOAO Proposal ID #2012B-0491
Hsiao E. Y. et al., 2015, A&A, 578, A9
Jeffery D. J., Branch D., 1990, in Wheeler J. C., Piran T., Weinberg S., eds, Supernovae, Jerusalem Winter School for Theoretical Physics. World Scientific Publ. Co., Singapore; Teaneck, NJ, p. 149

Jeffery D. J., Leibundgut B., Kirshner R. P., Benetti S., Branch D., Sonneborn G., 1992, ApJ, 397, 304
Jeffery D. J., Branch D., Baron E., 2006, preprint (astro-ph/0609804)
Jeffery D. J., Ketchum W., Branch D., Baron E., Elmhamdi A., Danziger I. J., 2007, ApJS, 171, 493
Jha S., Riess A. G., Kirshner R. P., 2007, ApJ, 659, 122
Kasen D., 2006, ApJ, 649, 939
Kasen D., Plewa T., 2007, ApJ, 662, 459
Kasen D., Woosley S. E., 2007, ApJ, 656, 661
Keenan P. C., 1984, in Garrison R. F., ed., The MK Process and Stellar Classification. Univ. Toronto, Canada, p. 29
Kerzendorf W. E., Sim S. A., 2014, MNRAS, 440, 387
Kessler R. et al., 2009, ApJS, 185, 32
Kewley L. J., Dopita M. A., 2002, ApJS, 142, 35
Kewley L. J., Ellison S. L., 2008, ApJ, 681, 1183
Khan R., Stanek K. Z., Stoll R., Prieto J. L., 2011, ApJ, 737, L24
Khokhlov A. M., 1991, A&A, 245, L25
Khokhlov A., Mueller E., Hoeflich P., 1993, A&A, 270, 223
Kim A. G. et al., 2014, ApJ, 784, 51
Kirshner R. P., Oke J. B., Penston M. V., Searle L., 1973, ApJ, 185, 303
Kirshner R. P. et al., 1993, ApJ, 415, 589
Kistler M. D., Stanek K. Z., Kochanek C. S., Prieto J. L., Thompson T. A., 2013, ApJ, 770, 88
Kobayashi C., Nomoto K., 2009, ApJ, 707, 1466
Kromer M. et al., 2013, ApJ, 778, L18
Lentz E. J., Baron E., Branch D., Hauschildt P. H., Nugent P. E., 2000, ApJ, 530, 966
Li W. D. et al., 1999, AJ, 117, 2709
Li W. et al., 2011, MNRAS, 412, 1441
Lira P. et al., 1998, AJ, 115, 234
Liu W., Jeffery D. J., Schultz D. R., 1997, ApJ, 483, L107
Liu W., Jeffery D. J., Schultz D. R., 1998, ApJ, 494, 812
Liu Z.-W., Moriya T. J., Stancliffe R. J., Wang B., 2015, A&A, 574, A12
McCully C. et al., 2014a, Nature, 512, 54
McCully C. et al., 2014b, ApJ, 786, 134
McGaugh S. S., 1991, ApJ, 380, 140
Maeda K., Kawabata K., Li W., Tanaka M., Mazzali P. A., Hattori T., Nomoto K., Filippenko A. V., 2009, ApJ, 690, 1745
Maeda K. et al., 2010, Nature, 466, 82
Maeda K., Kutsuna M., Shigeyama T., 2014, ApJ, 794, 37
Maguire K. et al., 2012, MNRAS, 426, 2359
Maguire K. et al., 2014, MNRAS, 444, 3258
Maguire K., Taubenberger S., Sullivan M., Mazzali P. A., 2015, preprint (arXiv:1512.07107)
Marion G. H. et al., 2015, ApJ, 798, 39
Maund J. R. et al., 2010, ApJ, 725, L167
Maurer I., Mazzali P. A., Taubenberger S., Hachinger S., 2010, MNRAS, 409, 1441
Mazzali P. A., Danziger I. J., Turatto M., 1995, A&A, 297, 509
Mazzali P. A., Sauer D. N., Pastorello A., Benetti S., Hillebrandt W., 2008, MNRAS, 386, 1897
Mazzali P. A. et al., 2014, MNRAS, 439, 1959
Mazzali P. A. et al., 2015, MNRAS, 450, 2631
Miles B. J., van Rossum D. R., Townsley D. M., Timmes F. X., Jackson A. P., Calder A. C., Brown E. F., 2015, preprint (arXiv:1508:05961)
Milisavljevic D. et al., 2013, ApJ, 767, 71
Milisavljevic D. et al., 2015, ApJ, 799, 51
Milne P. A., Brown P. J., 2012, preprint (arXiv:1201.1279)
Milne P. A. et al., 2010, ApJ, 721, 1627
Milne P. A., Brown P. J., Roming P. W. A., Bufano F., Gehrels N., 2013, ApJ, 779, 23
Moll R., Raskin C., Kasen D., Woosley S. E., 2014, ApJ, 785, 105
Munari U., Henden A., Belligoli R., Castellani F., Cherini G., Righetti G. L., Vagnozzi A., 2013, na, 20, 30
Niino Y., Nagamine K., Zhang B., 2015, MNRAS, 449, 2706
Nomoto K., Iwamoto K., Suzuki T., Pols O. R., Yamaoka H., Hashimoto M., Hoflich P., van den Heuvel E. P. J., 1996, in van Paradijs J., van den Heuvel E. P. J., Kuulkers E., eds, Proc. IAU Symp. 165, Compact Stars in Binaries. Kluwer Academic Pub., Dordrecht, p. 119
Nordsieck K., 2012, in Hoffman J. L., Bjorkman J., Whitney B., eds, American Institute of Physics Conference Series, Vol. 1429, Am. Inst. Phys. Conf. Ser., Am. Inst. Phys., NJ, p. 248
Nugent P., Phillips M., Baron E., Branch D., Hauschildt P., 1995, ApJ, 455, L147
Nugent P. E. et al., 2011, Nature, 480, 344
Pakmor R., Kromer M., Taubenberger S., Sim S. A., Röpke F. K., Hillebrandt W., 2012, ApJ, 747, L10
Pan Y.-C. et al., 2014, MNRAS, 438, 1391
Pan Y.-C., Sullivan M., Maguire K., Gal-Yam A., Hook I. M., Howell D. A., Nugent P. E., Mazzali P. A., 2015, MNRAS, 446, 354
Parrent J. T., 2014, preprint (arXiv:1412.7163)
Parrent J. T., Howell D. A., 2012, Cent. Bur. Electron. Telegrams, 3174, 2
Parrent J., Branch D., Jeffery D., 2010, Astrophysics Source Code Library, record ascl:1010.055
Parrent J. T. et al., 2011, ApJ, 732, 30
Parrent J. T. et al., 2012, ApJ, 752, L26
Parrent J., Friesen B., Parthasarathy M., 2014, Ap&S, 351, 1
Parrent J. T., Milisavljevic D., Soderberg A. M., Parthasarathy M., 2015, preprint (arXiv:1505.06645)
Pastorello A. et al., 2007a, MNRAS, 376, 1301
Pastorello A. et al., 2007b, MNRAS, 377, 1531
Pereira R. et al., 2013, A&A, 554, A27
Pettini M., Pagel B. E. J., 2004, MNRAS, 348, L59
Phillips M. M., 1993, ApJ, 413, L105
Phillips M. M., Wells L. A., Suntzeff N. B., Hamuy M., Leibundgut B., Kirshner R. P., Foltz C. B., 1992, AJ, 103, 1632
Phillips M. M., Lira P., Suntzeff N. B., Schommer R. A., Hamuy M., Maza J., 1999, AJ, 118, 1766
Phillips M. M. et al., 2013, ApJ, 779, 38
Pignata G. et al., 2011, ApJ, 728, 14
Pinto P. A., Eastman R. G., 2000a, ApJ, 530, 744
Pinto P. A., Eastman R. G., 2000b, ApJ, 530, 757
Poznanski D., Prochaska J. X., Bloom J. S., 2012, MNRAS, 426, 1465
Prieto J. L. et al., 2007, preprint (arXiv:0706.4088)
Raskin C., Kasen D., 2013, ApJ, 772, 1
Raskin C., Kasen D., Moll R., Schwab J., Woosley S., 2014, ApJ, 788, 75
Rau A. et al., 2009, PASP, 121, 1334
Richardson D., Thomas R. C., Casebeer D., Blankenship Z., Ratowt S., Baron E., Branch D., 2001, BAAS, 33, 1428
Röpke F. K. et al., 2012, ApJ, 750, L19
Ruiz-Lapuente P., Lucy L. B., 1992, ApJ, 400, 127
Sanders N. E. et al., 2012a, ApJ, 758, 132
Sanders N. E., Caldwell N., McDowell J., Harding P., 2012b, ApJ, 758, 133
Sasdelli M., Mazzali P. A., Pian E., Nomoto K., Hachinger S., Cappellaro E., Benetti S., 2014, MNRAS, 445, 711
Sasdelli M. et al., 2015, preprint (arXiv:1512.06810)
Scalzo R. A. et al., 2010, ApJ, 713, 1073
Scalzo R. et al., 2012, ApJ, 757, 12
Scalzo R. et al., 2014a, MNRAS, 440, 1498
Scalzo R. A. et al., 2014b, MNRAS, 445, 30
Scalzo R. A., Ruiter A. J., Sim S. A., 2014c, MNRAS, 445, 2535
Schlafly E. F., Finkbeiner D. P., 2011, ApJ, 737, 103
Schmidt G. D., Weymann R. J., Foltz C. B., 1989, PASP, 101, 713
Shen K. J., Moore K., 2014, ApJ, 797, 46
Silverman J. M., Ganeshalingam M., Li W., Filippenko A. V., Miller A. A., Poznanski D., 2011, MNRAS, 410, 585
Silverman J. M. et al., 2013, MNRAS, 436, 1225
Silverman J. M., Vinkó J., Marion G. H., Wheeler J. C., Barna B., Szalai T., Mulligan B. W., Filippenko A. V., 2015, MNRAS, 451, 1973
Smith N. et al., 2015, MNRAS, 449, 1876
Soares D. S. L., de Souza R. E., de Carvalho R. R., Couto da Silva T. C., 1995, A&AS, 110, 371
Soker N., 2014, MNRAS, 444, L73
Springob C. M., Masters K. L., Haynes M. P., Giovanelli R., Marinoni C., 2007, ApJS, 172, 599

Stanishev V. et al., 2007, A&A, 469, 645
Stehle M., Mazzali P. A., Benetti S., Hillebrandt W., 2005, MNRAS, 360, 1231
Stritzinger M. et al., 2002, AJ, 124, 2100
Stritzinger M. D. et al., 2015, A&A, 573, A2
Sullivan M. et al., 2010, MNRAS, 406, 782
Tanaka M. et al., 2008, ApJ, 677, 448
Tanaka M. et al., 2010, ApJ, 714, 1209
Tanikawa A., Nakasato N., Sato Y., Nomoto K., Maeda K., Hachisu I., 2015, ApJ, 807, 40
Taubenberger S. et al., 2008, MNRAS, 385, 75
Taubenberger S. et al., 2011, MNRAS, 412, 2735
Taubenberger S. et al., 2013, MNRAS, 432, 3117
Taylor E. N. et al., 2011, MNRAS, 418, 1587
Theureau G., Bottinelli L., Coudreau-Durand N., Gouguenheim L., Hallet N., Loulergue M., Paturel G., Teerikorpi P., 1998, A&AS, 130, 333
Thomas R. C., Branch D., Baron E., Nomoto K., Li W., Filippenko A. V., 2004, ApJ, 601, 1019
Thomas R. C. et al., 2007, ApJ, 654, L53
Thomas R. C., Nugent P. E., Meza J. C., 2011a, PASP, 123, 237
Thomas R. C. et al., 2011b, ApJ, 743, 27
Toonen S., Voss R., Knigge C., 2014, MNRAS, 441, 354
Valenti S. et al., 2014, MNRAS, 438, L101
van Dokkum P. G., Abraham R., Merritt A., 2014, ApJ, 782, L24
van Kerkwijk M. H., Chang P., Justham S., 2010, ApJ, 722, L157
van Rossum D. R., 2012, preprint (arXiv:1208.3781)
van Rossum D. R., Kashyap R., Fisher R., Wollaeger R. T., Garcia-Berro E., Aznar-Siguan G., Ji S., Loren-Aguilar P., 2015, preprint (arXiv:1510.04286)
Wang X. et al., 2009a, ApJ, 697, 380
Wang X. et al., 2009b, ApJ, 699, L139
Wang X. et al., 2012, ApJ, 749, 126
Wang X., Wang L., Filippenko A. V., Zhang T., Zhao X., 2013, Science, 340, 170
Wheeler J. C., Johnson V., Clocchiatti A., 2015, MNRAS', 450, 1295
Woosley S. E., Kasen D., 2011, ApJ, 734, 38
Woosley S. E., Weaver T. A., 1994, ApJ, 423, 371
Yamanaka M. et al., 2009, ApJ, 707, L118
Yaron O., Gal-Yam A., 2012, PASP, 124, 668
Zheng W. et al., 2013, ApJ, 778, L15

This paper has been typeset from a TEX/LATEX file prepared by the author.